molecules

MDPI

Review

Advances for Triangular and Sandwich-Shaped All-Metal Aromatics

Miaomiao Wang and Yanlan Wang *

Department of Chemistry and Chemical Engineering, Shandong Provincial Key Laboratory of Chemical Energy Storage and Novel Cell Technology, Liaocheng University, Liaocheng 252059, China; wmm_0214@163.com
* Correspondence: wangyanlan@lcu.edu.cn

Abstract: Much experimental work has been contributed to all-metal σ, π and δ-aromaticity among transition metals, semimetallics and other metals in the past two decades. Before our focused investigations on the properties of triangular and sandwich-shaped all-metal aromatics, A. I. Boldyrev presented general discussions on the concepts of all-metal σ-aromaticity and σ-antiaromaticity for metallo-clusters. Schleyer illustrated that Nucleus-Independent Chemical Shifts (NICS) were among the most authoritative criteria for aromaticity. Ugalde discussed the earlier developments of all-metal aromatic compounds with all possible shapes. Besides the theoretical predictions, many stable all-metal aromatic trinuclear clusters have been isolated as the metallic analogues of either the σ-aromatic molecule's $[H_3]^+$ ion or the π-aromatic molecule's $[C_3H_3]^+$ ion. Different from Hoffman's opinion on all-metal aromaticity, triangular all-metal aromatics were found to hold great potential in applications in coordination chemistry, catalysis, and material science. Triangular all-metal aromatics, which were theoretically proved to conform to the Hückel (4n + 2) rule and possess the smallest aromatic ring, could also play roles as stable ligands during the formation of all-metal sandwiches. The triangular and sandwich-shaped all-metal aromatics have not yet been specifically summarized despite their diversity of existence, puissant developments and various interesting applications. These findings are different from the public opinion that all-metal aromatics would be limited to further applications due to their overstated difficulties in synthesis and uncertain stabilities. Our review will specifically focus on the summarization of theoretical predictions, feasible syntheses and isolations, and multiple applications of triangular and sandwich shaped all-metal aromatics. The appropriateness and necessities of this review will emphasize and disseminate their importance and applications forcefully and in a timely manner.

Keywords: all-metal aromaticity; coordination; catalysis

Citation: Wang, M.; Wang, Y. Advances for Triangular and Sandwich-Shaped All-Metal Aromatics. *Molecules* **2024**, *29*, 763. https://doi.org/10.3390/molecules29040763

Academic Editor: Frantisek Hartl

Received: 26 December 2023
Revised: 19 January 2024
Accepted: 26 January 2024
Published: 7 February 2024

1. Introduction

The definition for aromaticity was originally proposed in the 19th century when August Kekulé proposed the typical structure of benzene, C_6H_6 [1–3]. Since then, aromaticity has become a popular concept and was wildly used in organic chemistry to demonstrate molecules possessing conjugated (4n + 2) π electrons. After vigorous and long development, this concept has been extended to numerous unsaturated organic species including the smallest cyclopropenyl cation and much larger polycyclic aromatics [4]. All-metal aromatics are a group of metallic rings that also conform to the Hückel (4n + 2) electrons rule. Depending on the type of electrons (s, p or d) delocalized among the metallic core, these all-metal aromatics possess σ, π or δ-aromaticity, respectively. More recently, the voice that the concept of aromaticity should not be extended beyond carbon-based systems is present because they believe that aromatic organometallics are very likely to be fragile. However, the discovery of all-metal aromaticity started from the theoretical predictions of aromaticity for metallocyclopentadienyls [5–10]. Later on, several organometallic compounds consisting of metallic aromatic rings have been isolated with fully qualified characterizations [11–13]. Before the vivant investigations on triangular all-metal aromatics,

A. I. Boldyrev presented general standards to identify the presence of all-metal aromaticity and antiaromaticity [3,14,15]. Meanwhile, Schleyer introduced Nucleus-Independent Chemical Shifts (NICS) in several papers and established a mature system to predict or prove aromaticity by this method [16–18]. Ugalde reviewed the earlier developments of all-metal aromatic compounds and encouraged their promising prospects for further utilization [19]. Later on, the advances in all-metal aromaticity were driven forcefully by several groups [20–23]. However, we are going to pay more attention to triangular all-metal aromatics and specifically summarize these group of organometallics due to its multiple theoretical predictions and existences, rapid developments and exciting application potentials [24,25].

Triangular all-metal aromatics are a group of organometallic complexes that conform to the Hückel (4n + 2) π electrons rule and contain the smallest metallic ring core. In fact, before the successful syntheses and isolation for solid-state triangular all-metal complexes, a great amount of work on theoretical calculations has already predicted the existence of triangular all-metal σ, π or δ-aromaticity among transition metals, semimetallics and other metals, even before 2010 [26–33]. Besides the theoretical predictions, all-metal aromaticity in stable trinuclear clusters has been disclosed by many chemists and these metallic clusters were proved to be either analogues of the σ-aromatic molecule's $[H_3]^+$ ion [34] or analogues of the π-aromatic molecule's $[C_3H_3]^+$ ion (Scheme 1) [35]. Besides the triangles, the discovery of aromaticity in four-membered all-metal clusters, like $[Al_4]^{2-}$, also showed considerable research activities [36,37].

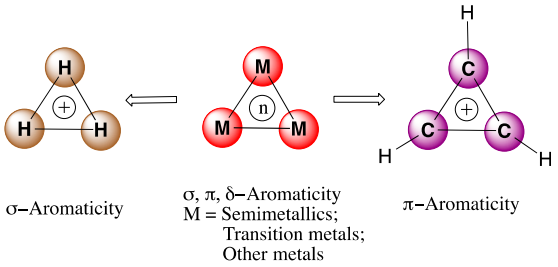

Scheme 1. Triangular all-metal aromatic clusters as metallic analogues of σ-aromatic molecule's $[H_3]^+$ ion or the π-aromatic molecule's $[C_3H_3]^+$ ion.

Here, in this review, we focus on the theoretical prediction and feasible synthesis of all types of present triangular and sandwich-shaped all-metal aromatics and their rapidly developing applications. The appropriateness of this summarization will boost the developments and applications of this new family of all-metal aromatics and debate Hoffman's opinion on all-metal aromaticity [38]. We found all-metal aromatics showed a range of potential applications which differ from the public's misunderstanding that they would be only the laboratory curiosity with gorgeous X-ray structures and limited to further utilizations due to their exaggerated complicated syntheses and low stabilities. As we know, even with the largest ring strain, the simplest aromatic molecular cyclopropenium ion $[C_3H_3]^+$ is quite stable and most of its metallic analogues showed comparable stabilities. All the known triangular all-metal aromatics will be presented and discussed below, mainly including the syntheses, characterizations and theoretical calculations of isolated triangular all-metal aromatic clusters, predictions of aromaticity in structures theoretically proposed, and their varieties of applications in coordination chemistry, catalytic reactions, and material sciences.

2. Experimental Findings of Triangular All-Metal Aromatic Clusters

2.1. Triangular π-Aromatic $[M_3]^{2-}$ (M = B, Al, Ga)

Group 13 triangular all-metal aromatics, which all possess three-centre-two-electron cores, are the earliest investigated triangular systems with aromaticity. In 1995, Robinson and co-workers reported the preparation of cyclogallene, $Na_2[(Mes_2C_6H_3)Ga]_3$

(Mes = 2,4,6-$Me_3C_6H_2$), which was the first isolated triangular all-metal aromatics. In this large organometallics, three gallium atoms were located on the three termini of the triangular ring core (Scheme 2) [39]. According to the crystal structure solved by X-ray diffraction, Na_2Ga_3 exhibited as a peculiar metallic trigonal bipyramid. The metallic core Na_2Ga_3 was arranged as two sodium atoms positioned above and beneath the $[Ga_3]^{2-}$ plane with the bond lengths measured as Ga–Ga: 2.441(1)Å and Ga–Na: 3.220(2) Å, respectively. The authors claimed that the gallium atoms are mainly sp^2 hybridized according to the electronic properties of cyclogallenes. There was one unoccupied p orbital left for each gallium atom without participating in the formation of a sigma bond. So, each of the two sodium atoms could donate one electron to the unoccupied p orbitals of the gallium atoms to provide the two 2π-electrons delocalized on three centres which are required for Hückel's (4n + 2) rule for the determination of aromaticity. Later, more groups found that group 13 M(I) metals could form cationic clusters easily via disproportionation reactions [40].

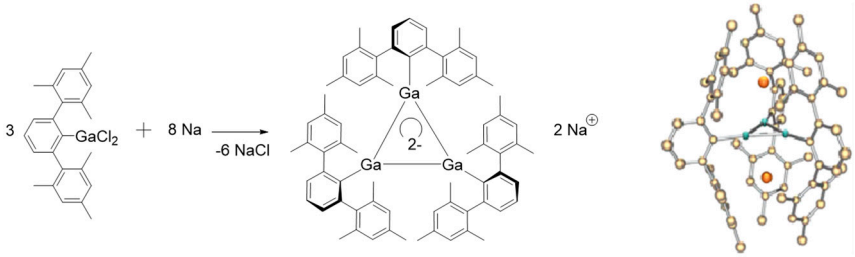

Scheme 2. Simple synthesis and X-ray structure of stable $[R_3Ga_3]^{2-}$ (R = $Mes_2C_6H_3$). Hydrogen atoms have been omitted. Adapted with permission from ref. [39] Copyright © 2024, American Chemical Society.

Besides experimental proof, theoretical calculations have been implemented in order to prove the existence of metalloaromaticity in the metallic ring dianion $[Ga]_3^{2-}$. Through investigation into their electron clouds (Figure 1) [41], the authors certificated that cyclogallenes were metallic analogues of the smallest main group triangular aromatic structure: cyclopropenium cation. The HOMO-1 of the cyclogallene in $Na_2[Ga_3H_3]$ presented extreme similarities to the π-electron cloud of the triangular aromatic $[C_3H_3]^+$ and also possessed the same number of valence electrons. Given the fully recognized "aromatic" property of the cyclopropenium cation, the authors believed that it was justified to claim that triangular "all-metal aromaticity" appeared in these cyclogallene dianions. Combining these experimental findings with their theoretical investigations, Robinson concluded that their isolated $Na_2[Ga_3H_3]$ was the first triangular all-metal π-aromatic structure.

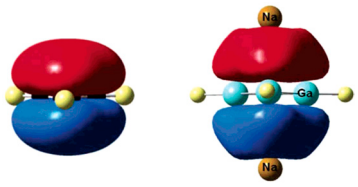

Figure 1. The π-electron clouds (HOMO-1) of the smallest aromatic ring $[C_3H_3]^+$ and its metallic analogue $Na_2[Ga_3H_3]$. Adapted with permission from ref. [41] Copyright © 2024, American Chemical Society.

Shortly after the introduction of $Na_2[(Mes_2C_6H_3)Ga]_3$, Robinson and co-workers reported the efficient synthesis and full characterizations of its analogous potassium complex $K_2[(Mes_2C_6H_3)Ga]_3$ (Equation (1)) [42] through the reaction of the corresponding gallium resource with potassium in 2007. K_2Ga_3 also contains a similar $[Ga_3]^{2-}$ aromatic core and bears typical organic ligands. The crystal structure showed that the mean Ga–Ga–Ga bond angle is nearly 60.0° and the Ga–Ga bond distances ranged from 2.4187(5) to 2.4317(5) Å.

$$3(Mes_2C_6H_3)GaCl_2 + 8K \rightarrow K_2[((Mes_2C_6H_3)Ga)]_3 + 6KCl \quad (1)$$

Quantum mechanical self-consistent field and density functional theory (DFT) were authoritative theoretical calculation tools and were exploited to theoretically examine the structural properties of the anionic cores $[Ga_3]^{2-}$, $[GaH]_3^{2-}$, $Na_2[GaH]_3$ and $K_2[GaH]_3$. Through full optimizations of their well-defined π molecular orbitals, they found these organometallic species were aromatic, as their calculated Independent Chemical Shifts (NICS) indices were largely negative. With solid experimental and theoretical results, they proved that the triangular metallic cyclogallene dianion, $[Ga_3]^{2-}$, exhibited definite aromatic behavior [43]. Robinson's group also proposed that when these three-membered rings were composed of mixed carbon, silicon atoms with gallium atoms could contribute heterocyclic 2π-electron cyclogallene systems which should also be synthetically accessible, stable, and aromatic [44]. Then, based on their huge amount of work in gallium-involved compounds, Robinson summarized short reviews in this field in which quite scientific comments were given on the structures and properties of triangular aromatic organometallic clusters [45].

In 2006, the Na_2Al_3 complex, which was an aluminium analogue for the cyclogallenes M_2Ga_3 (M = Na, K), was successfully isolated and theoretically demonstrated [46]. Through the rapid reduction process of $RAlI_2$ (R = $Mes_2C_6H_3$) using sodium metal, the three-aluminium core Na_2Al_3 was formed in diethyl ether and was successfully isolated after regular work up. According to the Kohn–Sham orbital representation for the delocalized HOMO-2 of Na_2Al_3 (Figure 2), the three aluminium atoms in Na_2Al_3 could also be considered as sp^2 hybridized, which was the same mode for the gallium atoms in cyclogallenes. X-ray structure of Na_2Al_3 showed the bond length of Al–Al was equal to 2.5202(2) Å on average in the aluminium ring core. Thus, Na_2Al_3 was the first characterized aromatic cycloaluminium complex.

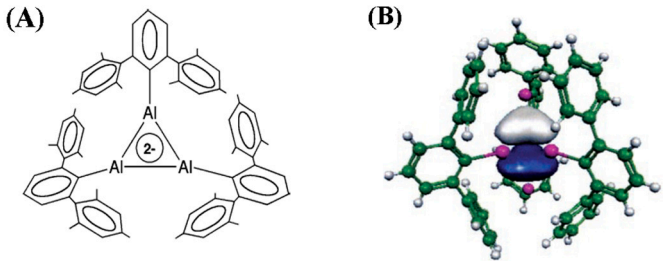

Figure 2. (**A**) The first isolated triangular 2π-electron metalloaromatic aluminium ring Na_2Al_3. (**B**) Kohn–Sham orbital representation for the delocalized HOMO-2 of Na_2Al_3. Adapted with permission from ref. [46] Copyright © 2024, Wiley-VCH Verlag GmbH & Co. KGaA, Weinheim, Germany.

Besides the heavier elements in group 13, the synthesis for the triboracyclopropenyl dianion was also reported in 2015. The boron-based analogue of the aromatic cyclopropenyl cation belongs to the prototypical Hückel π romatics. $[B_3(NCy_2)_3]^{2-}$ was isolated as its dimeric Na^+ salt $(Na_4[B_3(NCy_2)_3]_2$ (Figure 3A) [47], which was obtained through reduction of Cl_2BNCy_2 by sodium metal. Cyclic voltammetry measurements presented an extremely high oxidation potential (E_{pc} = −2.42 V), which was contributed by its good reactivity. The Hückel-type π aromatic character of the $[B_3(NCy_2)_3]^{2-}$ dianion was characterized by single-crystal X-ray diffraction and verified by various theoretical methods. DFT measurements clearly indicated the π aromaticity of the $[B_3]^{2-}$ core in a similar magnitude to that in cyclopropenium and benzene. In addition, the different ligands stabilized boron-based analogue $(B_3N_3Ph_6)^{2-}$ was synthesized by the simple reduction of $B_3N_3Ph_6$ using either potassium or rubidium in the 18-crown-6 ether. Similarly, DFT indicated that two electrons delocalized over the three boron atoms in the triangular $(B_3N_3Ph_6)^{2-}$, and the tri-boron core exhibited (π, σ)-mixed homoaromaticity. The reduced $(B_3N_3Ph_6)^{2-}$ could also act as a robust two-electron reductant for unsaturated compounds in reduction reaction (Figure 3B) [48].

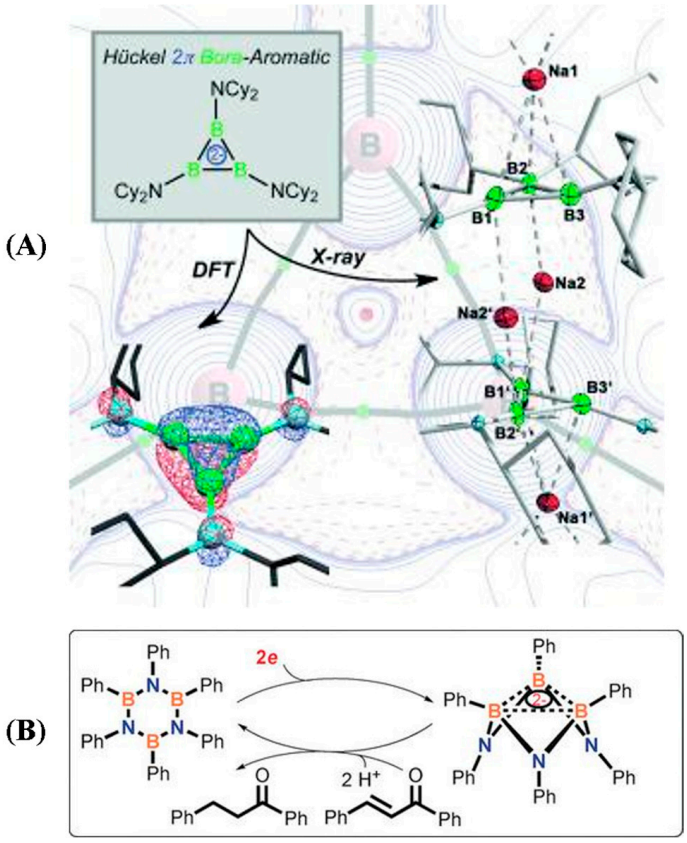

Figure 3. (**A**) The triboracyclopropenyl dianion $[B_3]^{2-}$: the lightest main-group-element Hückel π aromatic. Adapted with permission from ref. [48] Copyright © 2024, Wiley-VCH Verlag GmbH & Co. KGaA, Weinheim, Germany. (**B**) Aromatic trishomoaromatic $(B_3N_3Ph_6)^{2-}$ structure and its properties in two-electron reduction. Adapted with permission from ref. [48] Copyright © 2024, Wiley-VCH Verlag GmbH & Co. KGaA, Weinheim, Germany.

Besides the π-aromatic core $[B_3]^{2-}$, Frenking's group reported another smallest π-aromatic species B_3^+ in the $[B_3(NN)_3]^+$ and $[B_3(CO)_3]^+$ complexes in 2016. For comparison of the two representative 2π-aromatic systems, cyclic group-13 cation complex $[B_3L_3]^+$ featuring L→B dative bonds, and cyclic group-13 dianion $[B_3R_3]^{2-}$ featuring R-B electron-sharing bonds (Figure 4A) [49]. Spectroscopic identification (mass spectrum and experimental IR spectrum) was obtained for these boron–nitrogen cation complexes. The mass for these cations was formed through pulsed laser vaporization of a boron-11. Fully quantum chemical bonding analysis showed that the ligated adducts were mainly stabilized by the σ-donation of L→$[B_3L_2]^+$ (Figure 4B). This finding was a new field for ligand-stabilized boron complexes (B_3L_3), which could also be extended to main-group adducts with other atoms and ligands in three-membered cycles.

Furthermore, a noble-gas-supported aromatic B_3^+ cluster was also obtained by the contribution of strong covalent noble gas–boron bonds [50]. The triangular ion $[B_3]^+$ could also trap rare gases forming circular cationic compounds $B_3Rg_n^+$ [51]. In fact, besides the $[B_3]^{2-}$ and $[B_3]^+$ core, fully theoretical evidence confirmed the aromaticity in X_3^- (X = B, Al, Ga) species via Boldyrev's method [52]. Theoretical studies for the electronic structures, stabilities, and aromaticity in H_2B_2XH (X = N, P) molecules and the möbius aromatic planar metallaborocycles were also examined [53,54]. The above all-boron aromatic clusters could play important roles as potential novel ligands or building blocks in chemistry [55].

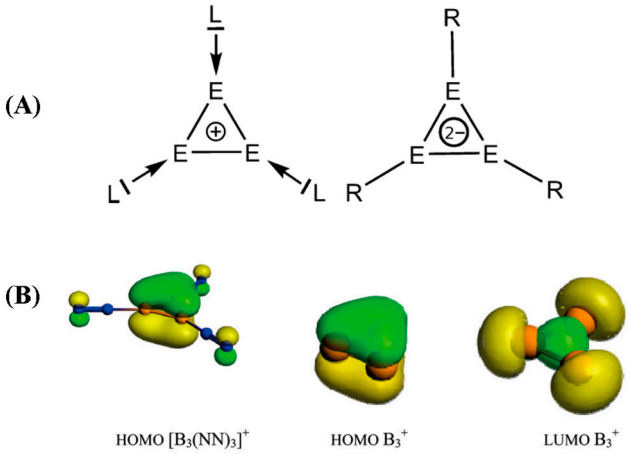

Figure 4. (**A**) Representative two 2π-aromatic systems: cyclic group-13 cation complex $[E_3L_3]^+$ (E = B) which featuring L→E dative bonds, and cyclic group-13 dianion which feature R-E electron-sharing bonds. (**B**) Plot of molecular orbitals using BP86/TZ2P+: HOMO for $[B_3(NN)^3]^+$, HOMO for $(X^1A_{1'})$ B_3^+ and LUMO for $(X^1A_{1'})$ B_3^+. Adapted with permission from ref. [49] Copyright © 2024, Wiley-VCH Verlag GmbH & Co. KGaA, Weinheim, Germany.

2.2. Triangular π-Aromatic $[Si]_3^+$, $[Ge]_3^+$, $[Si_2C]^+$

In addition to group 13 elements, cyclic cations $[A_3H_3]^+$ (A = C, Si, Ge, Sn, and Pb) were theoretically calculated with curiosities about whether these group of organometallics were going to show any evidence for aromaticity [56–58]. The experimental observation of three-membered cations made of the group 14 elements was predicted to be possible [59,60]. Soon, Sekiguchi and co-workers first reported the isolation and characterizations of new tris(tri-*tert*-butylsilyl)cyclotrigermenium tetraphenylborate $[t\text{-}Bu_3SiGe]_3^+BPh_4^-$, abbreviated as $[Ge_3]^+$ [61]. This $[Ge_3]^+$ system was a free germyl cation with 2π-electrons incorporated in the cyclic core. This $[Ge_3]^+$ complex could be isolated as a type of yellowish solid in the inert atmosphere after the reaction of tetrakis(tri-*tert*-butylsilyl)cyclotrigermene with trityl tetraphenylborate (Scheme 3A). The single-crystal X-ray crystallographic analysis for $[Ge_3]^+$ elucidated that Ge–Ge bond lengths range from 2.321(4) to 2.333(4) Å and the Ge–Ge–Ge bond angles vary from 59.8(1)° to 60.3(1)°. The three Ge atoms were localized in a nearly equilateral triangle. These crystallographic data resemble the cyclopropenium cation. The cyclotrigermenium cation $[Ge_3]^+$ prefers a planar existence due to the electronic properties and steric hindrance caused by the bulky *t*-Bu_3Si groups.

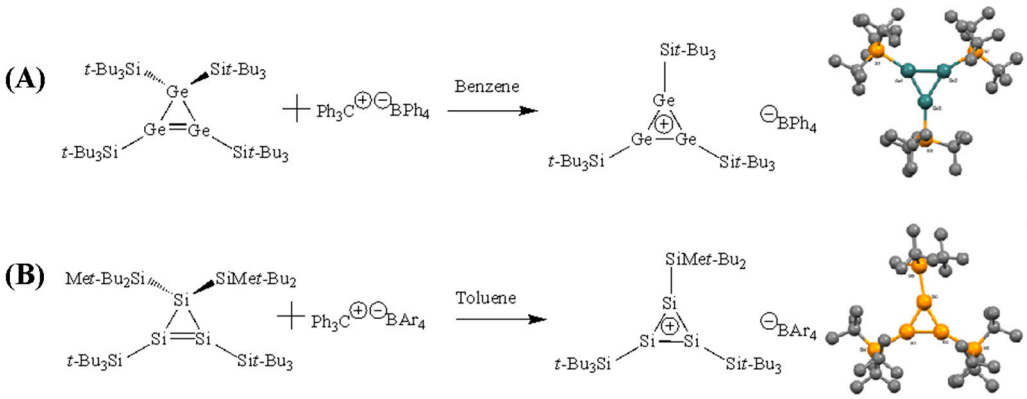

Scheme 3. (**A**) Synthesis and crystal structures of aromatic $(t\text{-}Bu_3SiGe)_3^+BPh_4^-$. (**B**) Synthesis and crystal structures of aromatic $[(t\text{-}Bu_3Si_2)_2(t\text{-}Bu_2MeSi_2)]^+BAr_4^-$. Counter anions, crystal solvent molecules and hydrogen atoms have been omitted for clarity (thermal ellipsoids are shown at 30% probability level). Adapted with permission from ref. [62] Copyright © 2024, American Chemical Society.

In 2005, the same group introduced the first isolation of the persilaaromatic structure $[(t\text{-}Bu_3Si_2)_2(t\text{-}Bu_2MeSi_2)]^+BAr_4^-$, abbreviated as $[Si_3]^+$ [62]. Due to the lack of proper precursors, the initial attempts for their syntheses were not successful. With modified methods in the presence of triphenylmethylium tetraarylborate, the desired cyclotrisilene was easily transformed into the targeted cyclotrisilenylium cation (Scheme 3B). According to the crystallographic data, the bond angles in the cyclotrisilenylium cation $[Si_3]^+$ range from 59.76(10)° to 60.20(10)° and the Si–Si bond lengths vary from 2.211(3) to 2.221(3) Å. The internal $[Si_3]^+$ core presented a nearly equilateral triangle. The three substituted silicon atoms are in the same plane within 0.39Å. These experimental characters of $[Si_3]^+$ hinted that it was another triangular all-metal aromatics made of semimetallics.

It is worth mentioning that the synthetic strategies for the robust heteroaromatic cluster $[Si_2C]^+$ were reported by Sekiguchi and co-workers based on the other group's previous investigations on their analogues [63]. Using $(t\text{-}Bu_3Si)_2SiLi_2$ and 1-adamantanecarbonyl chloride in polar organic solvent formed one yellow solid 1,1,2-tris(tri-*tert*-butylsilyl)-3-(1-adamantyl)disilacyclopropene, $[Si_2C]$, which was examined by X-ray crystallography. The hybridized $[Si_2C]$ included one Si=C double bond which was equal to 1.745(2) Å and these data resemble the simple cyclopropane. The reaction of $[Si_2C]$ with triphenylmethylium tetraarylborate gave 1,2-bis(tri-*tert*-butylsilyl)-3-(1-adamantyl) disilacyclopropenylium ion, $[Si_2C]^+$, with great isolated yield (Scheme 4). The tetraarylborate salt of $[Si_2C]^+$ was isolated as yellow crystals and was quite sensitive to air and water. The silicon–carbon hybridized $[Si_2C]^+$ complex represented the first isolable derivative of cyclopropenylium ion, $[C_3]^+$. The mixed heteroaromatic $[Si_2C]^+$ showed an isosceles triangle in crystal structures; similarly, both the cyclopropenyl cation $[C_3]^+$ and its silyl analogue $[Si_3]^+$ were arranged in equilateral triangular cores.

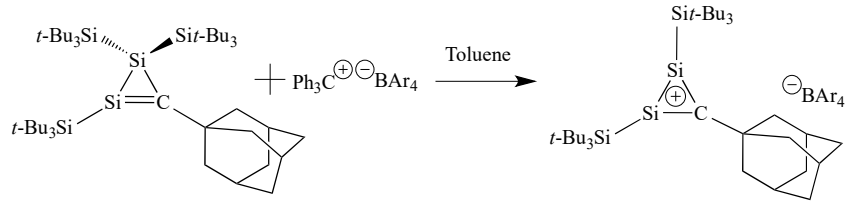

Scheme 4. Preparation of substituted $[Si_2C]^+$ by mixing functionalized $[Si_2C]$ with triphenylmethylium tetraarylborate in organic solvent. Adapted with permission from ref. [63] Copyright © 2024, American Chemical Society.

The first three-membered $TiSn_2$ ring core was also isolated and fully characterized in 2014 by Kuwabara and coworkers [64]. Normally, the Ti–Sn single bonds in coordinated complexes range from 2.842 to 2.984 Å. However, they found that the Ti–Sn bond lengths in $TiSn_2$ ranged from 2.6867(16) to 2.7254(17) Å for $Cp_2Ti[SnC_4Et_4]_2$, which was obviously shorter. In addition, the regular bond lengths for Sn=Sn bonds range from 2.575(4) to 2.85126(19) Å; however, the distance between the two Sn atoms in $TiSn_2$ was equal to 3.0576(14) Å, which was obviously much longer. All these crystal results implied the possibility of the presence of electron delocalization and aromaticity in the three-membered $TiSn_2$ core. Indeed, their following complementary theoretical analysis confirmed that their triangular $TiSn_2$ was σ-aromatic. Further, another niobium-necked cluster $[As_3Nb(As_3Sn_3)]^{3-}$ was also experimentally and theoretically examined, and confirmed that the Sn_3^{2-} core was aromatic [65].

2.3. Triangular σ-Aromatic $[Au]_3^+$

Using powerful N-heterocyclic carbene (NHC) 1,3-bis(2,6-diisopropylphenyl)imidazol-2-ylidene as the ligand, the first NHC-coordinated triangular tri-gold cluster $[LAu]_3^+$ was synthesized by Sadighi's group in 2012 [66]. The preparation of $[LAu]_3^+$ was quite simple, with two steps (Scheme 5). First, the monomer $[(LAu)_3CO_3]^+OTf^-$ was obtained when $[(LAu)_2OSiMe_3]^+OTf^-$ reacted with $[LAuOSiMe_3]$ under the pure CO_2 atmosphere.

Secondly, in the presence of CO, $[(LAu)_3CO_3]^+OTf^-$ underwent reduction and gave the reduced cyclic trimer, $[(LAu)_3]^+OTf^-$. Crystallographic analysis for triangular $[LAu]_3^+$ cation showed approximate D_3 symmetry with canted imidazolylidene rings (Figure 5a). The $[Au]_3^+$ ring was nearly equilateral, the Au–Au–Au bond angles ranged from 59.603(9)° to 60.331(8)° and the length of the Au–Au bond ranged from 2.6438(5) to 2.6633(5) Å. The three directly connected carbon atoms on the NHC are basically coplanar with the triangular $[Au]_3^+$ core.

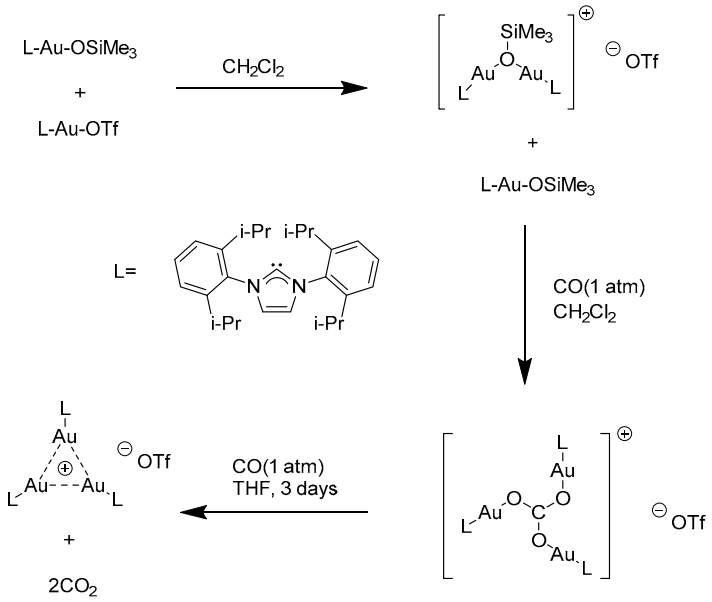

Scheme 5. Synthetic route for the cationic trigold(I) cluster and its following reduction to $[Au]_3^+OTf^-$. Adapted with permission from ref. [66] Copyright © 2024, Wiley-VCH Verlag GmbH & Co. KGaA, Weinheim, Germany.

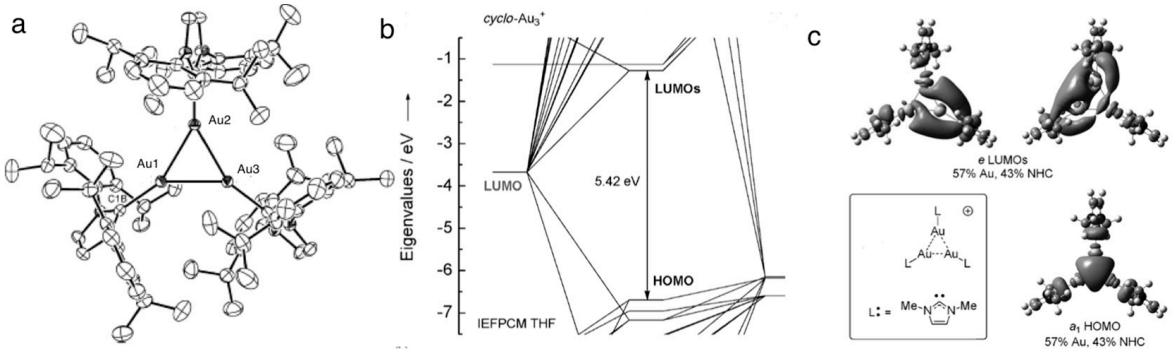

Figure 5. (**a**) Crystal structure of $[LAu]_3^+$ (L = 1,3-bis(2,6-diisopropylphenyl)imidazol-2-ylidene). Selected bond lengths [Å]: Au1–Au2 2.6563 (6), Au1–Au3 2.6633(5), Au2–Au3 2.6438(5); and bond angles [°]: Au2-Au1-Au3, 59.603(9), Au2-Au3-Au1, 60.066(15), Au3-Au2-Au1, 60.331(8). (**b**) The partial Kohn–Sham orbital energy diagram of $[LAu]_3^+$. (**c**) Plots of selected orbitals and percentage compositions based on electron densities for $[LAu]_3^+$. Adapted with permission from ref. [67] Copyright © 2024, Wiley-VCH Verlag GmbH & Co. KGaA, Weinheim, Germany.

Full valence delocalization along the cationic tri-gold core was discovered according to their complementary DFT analysis. The HOMO was composed mainly of the 6s orbitals for gold and the LUMO was composed of a degenerate pair. According to the frontier-orbital energy-level diagram, the calculated HOMO–LUMO gap was quite large (5.42 eV), which hinted at potential inert properties (Figure 5b). Theoretical parameters explained the great stabilities of the complex $[LAu]_3^+OTf^-$. The plots of the highest occupied (HOMO) and

the lowest unoccupied Kohn–Sham orbitals (LUMOs) showed their corresponding electron densities (Figure 5c). Their orbital pictures were analogous to that of aromatic $[H_3]^+$ and their frontier orbitals were echoed by those in $[H_3]^+$. So, this σ-aromatic $[Au_3]^+$ core with only 6s orbitals contributed to the necessary delocalized three-centre-two-electron mode was isolobal to σ-aromatic $[H_3]^+$.

In 2014, Bertrand's group improved the syntheses of aromatic $[LAu]_3^+$ species with different NHC ligands and attempted applying these peculiar tri-gold clusters in the regular catalytic carbonylation of amines in the presence of CO under mild conditions and presented somehow ordinary reactivities [67]. Based on the known Sadighi's synthetic strategies, Bertrand introduced another two straightforward synthetic routes for triangular aromatic gold complexes either ligated by three cyclic (alkyl)(amino)carbenes (CAAC) or by mixed ligands (two CAACs plus one phosphine). The first method was treatment of the $(CAAC_{c\text{-}Hex})AuCl$ with Ag_2O in the presence of $NaBF_4$ in a polar organic solvent. The intermediate complex $(CAAC_{c\text{-}Hex})_3Au_3O^+$ was obtained as an off-white solid. Then, this oxidized complex was reduced by CO, which yielded pale-yellow solid $(CAAC_{c\text{-}Hex})_3Au_3^+$, abbreviated as $[Au]_3^+$ (Scheme 6). The melting point of $[Au]_3^+$ was 240 °C (dec.), which was an indication of good stability. Indeed, the $[Au]_3^+$ cluster was tested to be robust to oxygen or water, which was an important advantage for further catalytic utilizations.

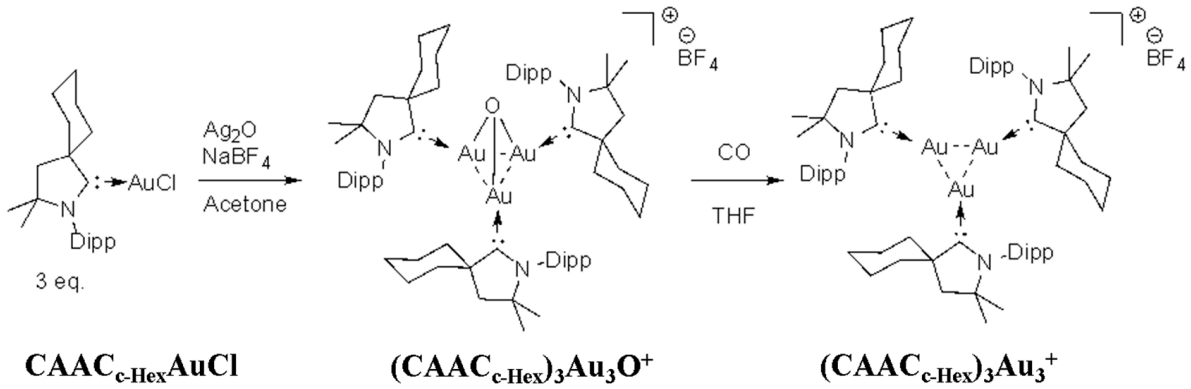

Scheme 6. Novel syntheses of trinuclear gold clusters $(CAAC_{c\text{-}Hex})_3Au_3O^+$ and $(CAAC_{c\text{-}Hex})_3Au_3^+$. Adapted with permission from ref. [67] Copyright © 2024, Wiley-VCH Verlag GmbH & Co. KGaA, Weinheim, Germany.

The phosphine/NHC ligand exchange possibilities were also investigated using the phosphine-supported μ^3-oxo cluster $(PPh_3)_3Au_3O^+$ as starting material (Scheme 7). Adding excess equivalents of $CAAC_{diEt}$ ligand to $(PPh_3)_3Au_3O^+$ gave the μ^3-oxo complex $(CAAC_{diEt})_3Au_3O^+$ with good isolated yield. The targeted trinuclear gold ring $(CAAC_{diEt})_3Au_3^+$ was obtained in nearly quantitative yield after a routine reduction process. When fewer equivalents of $CAAC_{diEt}$ were used, the mixed (CAAC)(phosphine)-ligated complex $(CAAC_{diEt})_2PPh_3Au_3^+$ was formed with a moderate yield.

According to the crystallographic analyses, the Au–Au distances in $CAAC_{diEt})_3Au_3^+$ ranged from 2.6324(8) to 2.6706(8) Å; however, the value was 3.1669(3)–3.3149(3) Å for its oxidized analogue. Comparing the Au–Au bond lengths for these two crystal structures, apparent bond length differences were found. Normally, true covalent bonds are hinted in $CAAC_{diEt})_3Au_3^+$ due to their unbelievably short metal–metal bond distances. What is worth mentioning is that the CAACs ligand showed stronger σ-donor properties than triphenyl phosphine in the mixed-ligand coordinated structure $(CAAC_{diEt})_2PPh_3Au_3^+$. This improved synthetic route provided possibilities for preparation of a variety of polynuclear gold (1/3 valence) clusters through ligand exchanges. Similar to Sadighi's structure, these mixed ligated clusters $[Au]_3^+$ should also be the analogues of σ-aromatic $[H_3]^+$.

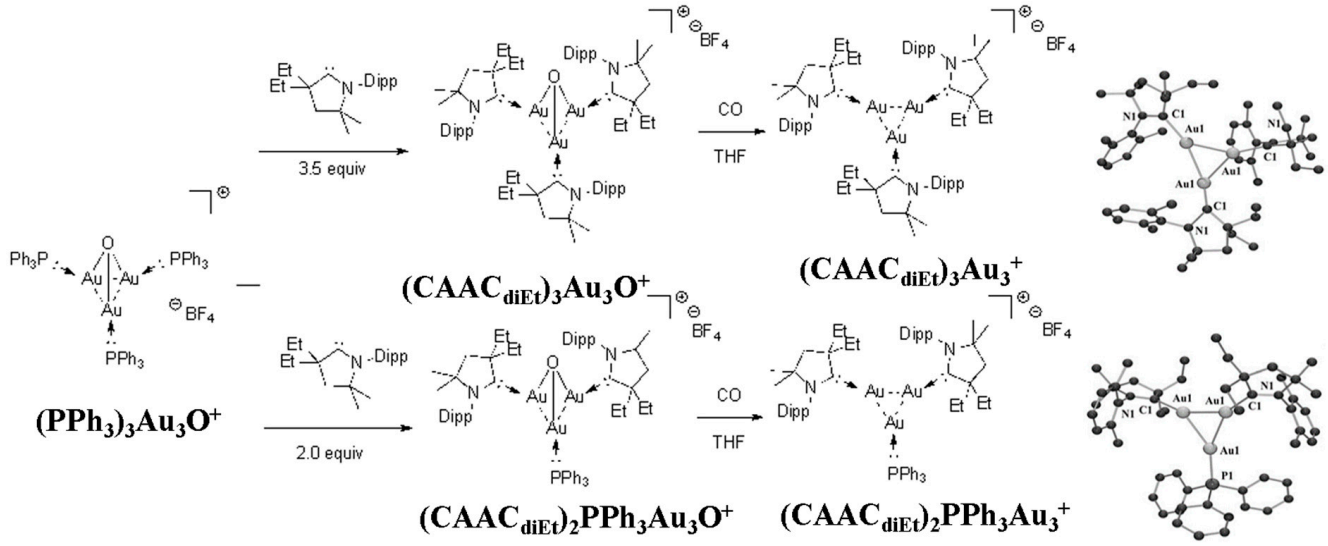

Scheme 7. Syntheses and crystal structures of triangular gold clusters $(CAAC_{diEt})_3Au_3^+$ and the mixed ligands stabilized $(CAAC_{diEt})_2PPh_3Au_3^+$. Adapted with permission from ref. [67] Copyright © 2024, Wiley-VCH Verlag GmbH & Co. KGaA, Weinheim, Germany.

2.4. Triangular σ-Aromatic $[Zn_3]^+$, $[Zn_2Cu]$

In 2015, the triangular all-metal aromaticity was extended to Zinc-involved systems by Frenking and Fischer's group. They synthesized and fully characterized the neutral triangular cluster $[Zn_2CuCp^*_3]$, abbreviated as $[Zn_2Cu]$ and the cationic cluster $[Zn_3Cp^*_3][BAr_4^F]$ (Cp^* = η-C_5Me_5), abbreviated as $[Zn_3]^+$ (Figure 6) [68]. The synthetic procedures were convenient by simply adding $[ZnCp^*]^+$ and $[CuCp^*]$ to [Cp*Zn-ZnCp*] (Carmona's compound) and stirring. The Zn–Zn bond in [Cp*Zn-ZnCp*] remained after the transformation to the final trimers. The authors claimed that using fluoroaromatic solvents was crucial for their efficient transformation. In addition, Fischer further reported the complementary experimental and theoretical investigations for the pseudo two-electron Cu/Zn clusters [69].

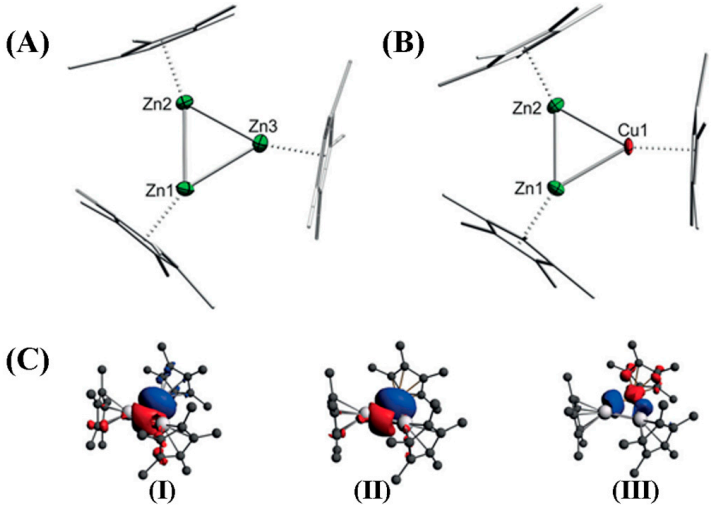

Figure 6. (**A**) Crystal structures of equilateral $[Zn_3]^+$; (**B**) Crystal structures of isosceles $[Zn_2Cu]$. (**C**) Deformation densities in triangular $[Zn_3]^+$ and $[Zn_2Cu]$. (**I**) $[Zn_2Cp^*_2]$ $[ZnCp^*]^+$ σ donation. (**II**) $[Zn_2Cp^*_2]$ $[CuCp^*]$ σ donation. (**III**) $[Zn_2Cp^*_2]$ $[CuCp^*]$ π back-donation. For better understanding, the direction of the charge flow was set from the red part to the blue part. Adapted with permission from ref. [68] Copyright © 2024, Wiley-VCH Verlag GmbH & Co. KGaA, Weinheim.

They crystalized both the $[Zn_3]^+$ and $[Zn_2Cu]$ clusters even sensitive properties were observed for these two ligated metallic trimers. Tri-zinc complex $[Zn_3]^+$ crystallized in the ordinary monoclinic space group $P2_1/c$ with two different formula units arranged together (Figure 6A). The neutral compound $[Zn_2Cu]$ crystallized in the typical triclinic space group P_1^- (Figure 6B). The bond angles for $[Zn_3]^+$ were very similar as 59.22(1)°, 59.71(2)° and 61.06(2)°, and for $[Zn_2Cu]$, the angles were measured as 59.33(2)°, 60.34(3)° and 60.34(3)°. So, the metal atoms in both three-membered core structures presented almost equilateral triangular arrangements. The average distance of Zn–Zn bond in $[Zn_3]^+$ was 2.430(1) Å. Similarly, the two Zn–Cu bonds in isosceles $[Zn_2Cu]$ were measured to be the same and was equal to 2.381(1) Å. The only Zn1–Zn2 bond in $[Zn_2Cu]$ was slightly shorter than 2.357(1) Å. All metal–metal bonds in these two complexes are slightly longer compared with their zinc-contained starting material decamethyldizincocene [70].

In order to better understand the bonding interactions of these two triangular clusters, the cationic $[Zn_3]^+$ and its neutral homologue $[Zn_2Cu]$ were calculated using the *meta*-GGA functional M06L method [71,72]. The nature of the bonding was analyzed by the energy decomposition analysis (EDA) method. They found that the σ donation of $[Zn_2]$ to $[Zn]^+$ into its empty 4s valence orbital was the main constitution for the overall orbital interactions (Figure 6C(I)). In addition, there are two types of leading orbital interactions for the neutral complex $[Zn_2Cu]$ including the σ-donation from $[Zn_2]$ to [Cu] and the π back-donation from [Cu] to $[Zn_2]$ (Figure 6C(II,III)). Both the triangular cores $[Zn_3]^+$ and $[Zn_2Cu]$ showed valence electrons (cve) delocalization in one cyclic plane and presented apparent implications for σ-aromaticity which was further confirmed by quantum chemical calculations. Similar to the triatomic hydrogen ion $[H_3]^+$, both the $[Zn_3]^+$ and $[Zn_2Cu]$ clusters revealed a high degree of *σ*-aromaticity.

2.5. Triangular Homoleptic $[Hg_3]^{4+}$

The homoleptic triangular cluster $[Hg_3(\mu\text{-dmpm})_4][O_3SCF_3]_4$ [dmpm = bis(dimethylphosphino)methane], abbreviated as $[Hg_3]^{4+}$ [73], was synthesized and crystalized by Peringer's group many years after their other brief report on a similar cluster, $[Hg_3(\mu\text{-dppm})_3][O_3SCF_3]_4$ [dppm = bis(diphenylphosphino)methane] [74]. Each of the mercury atom in the cluster $[Hg_3]^{4+}$ represented the 4/3 oxidation state. It was simply synthesized by mixing $[Hg_2]^{2+}$ with excess dmpm (Equation (2)) or by the reduction of $[Hg(Me_2SO)_6][O_3SCF_3]_2$ in the presence of dmpm and mercury (Equation (3)).

$$2[Hg_2][O_3SCF_3]_2 + 4\ dmpm \rightarrow [Hg_3(\mu\text{-dmpm})_4][O_3SCF_3]_4 + Hg \quad (2)$$

$$2[Hg(Me_2SO)_6][O_3SCF_3]_2 + 4\ dmpm + Hg \rightarrow [Hg_3(\mu\text{-dmpm})_4][O_3SCF_3]_4 + 12\ Me_2SO \quad (3)$$

According to the single-crystal X-ray analysis for complex $[Hg_3]^{4+}$ (Figure 7), this molecule was composed of four $CF_3SO_3^-$ anions for each $[Hg_3]^{4+}$ cation, so the oxidation state for each Hg was distributed as +4/3 correspondingly. The cationic $[Hg_3]^{4+}$ core was presented as a triangular mercury ring with bond lengths measured as Hg–Hg 276.68(14), 295.53(14) and 280.99(14) pm. There are four dmpm ligands involved for three mercury atoms, and the mercury edges are linked to either one or two phosphorous bridges. The three Hg atoms are nearly in a plane. Because of the intramolecular exchange between the two types of dmpm ligands, the complex showed fluxional ^{31}P NMR signals at 81 MHz at room temperature. According to the experimental parameters for homoleptic $[Hg_3]^{4+}$ cation, it was assumed to be another close analogue of the $[Au_3]^+$ and the $[Zn_3]^+$ systems, which are isolobal to σ-aromatic $[H_3]^+$.

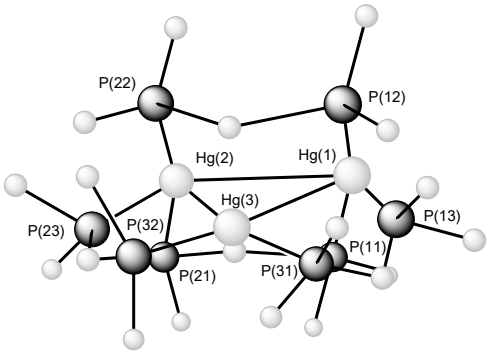

Figure 7. Crystal strucuture of homoleptic triangular $[Hg_3(\mu\text{-dmpm})_4]^{4+}$. Adapted with permission from ref. [73] Copyright © 2024, Royal Society of Chemistry.

2.6. Triangular δ-Aromatic $[Pd_3]^+$, $[Pt_3]^+$, $[Pd_2Pt]^+$, $[PdPt_2]^+$

In 2014, Malacria's group reported the mixed-ligand stabilized 44-cve tri-palladium cluster $[Pd_3(\mu_2\text{-SPh})_3(PPh_3)]^+$, abbreviated as $[Pd_3]^+$, as the first isolated *d*-block analogue of the π-aromatic cyclopropenyl cation $[C_3H_3]^+$ [75]. These $[Pd_3]^+$ clusters were firstly obtained by using S-aryl isothioureas as the sulfur source and have further been confirmed to be *δ*-aromatic by theoretical calculations (Scheme 8A). Then, a much-improved method was presented to access the identical tri-palladium cluster $[Pd_3]^+$ and its homoaromatics tri-platinum cluster $[Pt_3]^+$ and mixed-metallic heteroaromatics $[Pd_2Pt]^+$ and $[PdPt_2]^+$ (Scheme 8B) [76]. This new synthetic route was more efficient with almost quantitative conversions without preparing the S-aryl isothioureas. Using this updated method, aliphatic S-bridges and aliphatic phosphorous ligands are compatible and can be installed with high yields. The anionic part for the targeted $[Pd_3]^+$ cluster could be changed simply by hiring different Ag^I salts. By replacing disulfide with diselenides, the Se-bridged $[Pd_3]^+$ complex could also be obtained with much lower yields due to its intrinsic lower stabilities. The triangular triplatinum cluster $[Pt_3]^+$ could also be prepared using Pt^0 precursor $Pt(dba)_3$ instead of Pt^{II} species in order to achieve more efficient and more selective transformations [77]. Most importantly, when Pd(0) and Pt(0) precursors were mixed in 2:1 or 1:2 ratios, the peculiar heterobimetallic clusters $[Pd_2Pt]^+$ and $[PdPt_2]^+$ were formed, respectively (Figure 8). The isolated $[Pd_2Pt]^+$ and $[PdPt_2]^+$ clusters were considered the first confirmed triangular all-metal heteroaromatics among all the published Pd/Pt mixed complexes [78]. Both the heteroaromatic structures $[Pd_2Pt]^+$ and $[PdPt_2]^+$ were fully characterized including conclusive High Resolution Mass Spectroscopy (HRMS) and single-crystal X-ray diffraction (XRD).

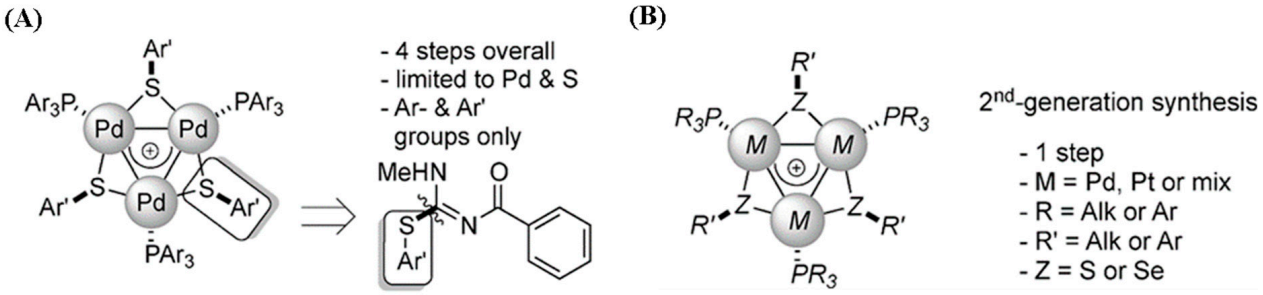

Scheme 8. Initial (**A**) and improved (**B**) synthetic routes for aromatic $[Pd_3]^+$, $[Pd_3]^+$ and heteroaromatics $[Pd_2Pt]^+$ and $[PdPt_2]^+$ clusters. Adapted with permission from ref. [76] Copyright © 2024, Wiley-VCH Verlag GmbH & Co. KGaA, Weinheim, Germany.

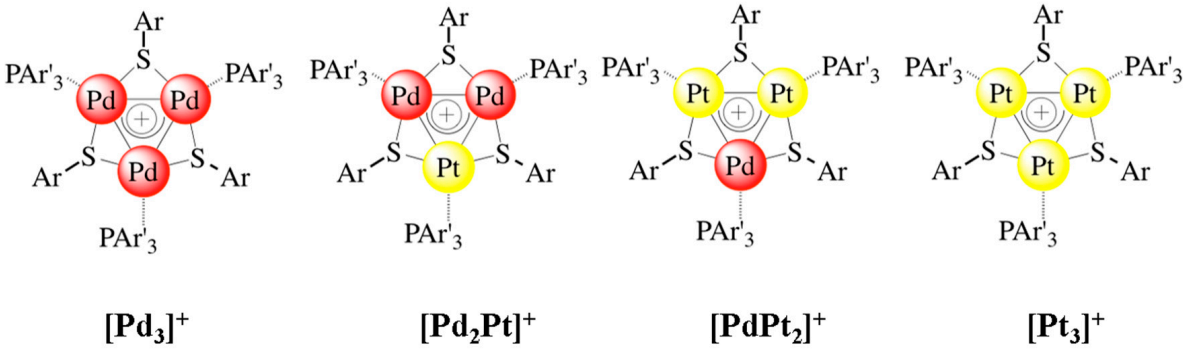

Figure 8. Representative examples for all-metal δ-aromatic triangular molecules $[Pd_3]^+$, $[Pt_3]^+$ and heteroaromatics $[Pd_2Pt]^+$, $[PdPt_2]^+$ in which Z = S, anion = SbF_6, R = 4-ClC_6H_4 and R′ = 4-FC_6H_4.

For better illustrations and comparisons of the four analogue clusters $[Pd_3]^+$, $[Pt_3]^+$, $[Pd_2Pt]^+$ and $[PdPt_2]^+$ in the X-ray analyses, identical substituent groups were chosen with anion = SbF_6, R = 4-FC_6H_4 and R′ = 4-ClC_6H_4, as presented in Figure 9A. After optimization, these four crystalline $[Pd_3]^+$, $[Pt_3]^+$, $[Pd_2Pt]^+$ and $[PdPt_2]^+$ remained triangular, quasi-symmetric structures without any symmetry constraints. Their triangular all-metal core was found to be nearly D_{3h}-symmetric and their whole structure was almost C_3 symmetry for all these four complexes. The homometallic $[Pd_3]^+$ and $[Pt_3]^+$ triangles were always found to be perfectly equilateral with identical bond angles (60.0°) and exactly the same metal–metal bond lengths no matter the various substituted groups and anions. The Pd–Pd bond distance in $[Pd_3]^+$ core equalled 2.8731(8) Å and the Pt–Pt length in $[Pt_3]^+$ core was 2.8690(4) Å. These data were generally below the sum of Van der Waals radii (3.26 Å).

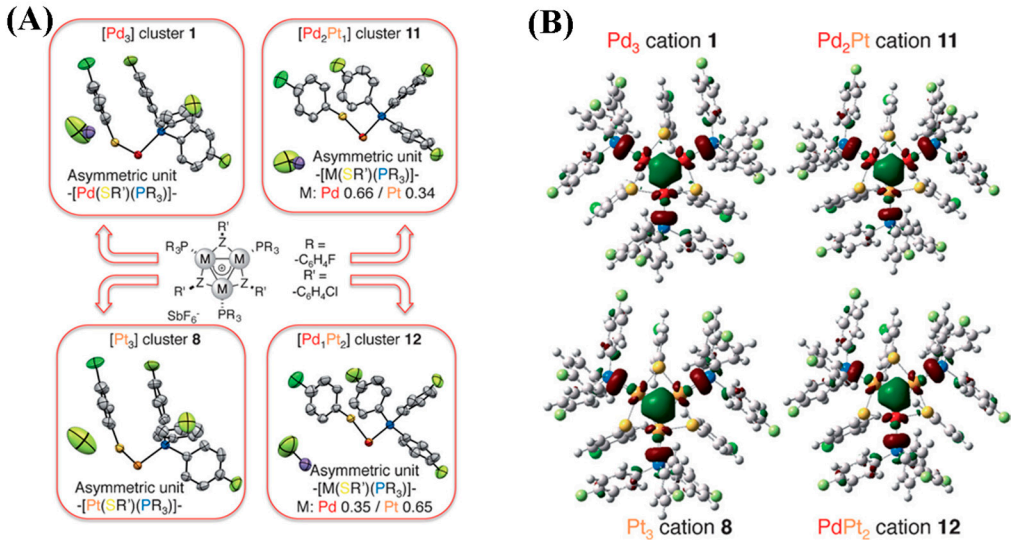

Figure 9. (**A**) Crystallographic comparison for metallic clusters $[Pd_3]^+$, $[Pt_3]^+$ and bimetallic $[Pd_2Pt]^+$ and $[PdPt_2]^+$. (**B**) Delocalized HOMOs for metallic clusters $[Pd_3]^+$ and $[Pt_3]^+$ and bimetallic clusters $[Pd_2Pt]^+$ and $[PdPt_2]^+$. Adapted with permission from ref. [76] Copyright © 2024, Wiley-VCH Verlag GmbH & Co. KGaA, Weinheim, Germany.

For the heteroaromatic complexes $[Pd_2Pt]^+$ and $[PdPt_2]^+$, 35% Pd and 65% Pt in $[PdPt_2]^+$ and 66% Pd and 34% Pt in $[Pd_2Pt]^+$ were presented in proportions. The bond angles in these heteroaromatic analogues deviated from 59.5(5) to 60.5(6)°. The averaged bond distance is 2.86(3) Å in $[PdPt_2]^+$ and 2.87(4) Å in $[Pd_2Pt]^+$. These parameters were very close to their homonuclear complexes $[Pd_3]^+$ and $[Pt_3]^+$. Because of the lanthanide contraction, the atomic radii for Pt and Pd are nearly equalized. So, the metal–metal

distances are alike for the heterobimetallic clusters $[Pd_2Pt]^+$ and $[PdPt_2]^+$. However, the situation would be much different when two main-group elements were combined.

The most characteristic molecular orbitals for complexes $[Pd_3]^+$, $[Pt_3]^+$, $[Pd_2Pt]^+$ and $[PdPt_2]^+$ were analyzed and compared (Figure 9B). Interestingly, identical bonding HOMOs were found for these four analogues complexes. Not surprisingly, the two bimetallic complexes $[Pd_2Pt]^+$ and $[PdPt_2]^+$ presented reasonable sigmoidal symmetry properties. There is clearly a three-centre-two-electron bond delocalized in their HOMOs. In addition, not only the HOMO but also HOMO-6 and HOMO-36 showed many similarities with the other early transition metal complexes in which *d*-orbital and *δ*-aromatic properties were confirmed through molecular orbitals calculations.

Indeed, the presence of *d*-orbital aromaticity with a typical delocalized three-centre-two-electron bond among the three-membered metallic ring cores of $[Pd_3]^+$, $[Pt_3]^+$, $[Pd_2Pt]^+$ and $[PdPt_2]^+$ was further confirmed by natural bond orbital (NBO) analyses [79] and adaptive natural density partitioning (AdNDP) results [80]. The chemical shifts for these four clusters were always negative (5 Å) in the NICS analyses, which was also a characteristic phenomenon for aromatic structures. The delocalization state of the cyclic electron was also proved by magnetic susceptibilities obtained by SQUID measurements [81,82]. Normally, the χT for a non-aromatic, quasi-symmetric, triangular cluster, $[Pd(CO)PPh_3]_3$ equals 0.04 emuKmol^{-1} at 300 K. This value was 0.44 emuKmol^{-1} for $[Pd_3]^+$ and 0.48 emuKmol^{-1} for $[Pt_3]^+$, respectively, under identical conditions. However, the susceptibilities for bimetallic complexes $[Pd_2Pt]^+$ and $[PdPt_2]^+$ were somehow as low as 0.22 and 0.26 emuKmol^{-1}, respectively, which was reasonable, because heteroarenes normally show much lower diamagnetic susceptibilities than their analogues homoarenes, even for the molecules made of main group elements [83]. In any case, all four complexes showed much higher values than those of ordinary non-aromatic clusters. The above experimental and theoretical proofs are fully consistent with the presence of *δ*-aromaticity for this group of triangular all-metal aromatics.

2.7. Triangular Heteroaromatic $[Pd_2Ru]^+$

More recently, with the development and increasing interest in the fields of all-metal triangular aromatics, A. I. Boldyrev and coauthors presented another ligand-stabilised heterobimetallic triangular compound $[Pd_2Ru]^+$ (Figure 10) [84]. This complex was air-stable and definitely was the first all-metal aromatic structure composed of noble metals Pd and Ru. Through structural and theoretical analyses, the authors demonstrated both similarities and differences for $[Pd_2Ru]^+$ compared to its parental $[Pd_3]^+$. Indeed, AdNDP and magnetic criteria proved that the $[Pd_2Ru]^+$ core presented obvious overlap between the d_{z^2} AO of ruthenium and the d_{xy} or d_{x^2}—$_{y2}$ AOs of the other two palladium atoms. So, the comprehensive characterisations proved that there is σ-aromaticity among the metal triangular core $[Pd_2Ru]^+$.

However, this structure was actually a byproduct of the reaction to obtain the expected metal triangle $[PdRu_2]^+$ according to the ratio for the two metallic starting reagents. Notably, the two Pd atoms were coordinated with triaryl phosphines, the unique Ru atom was coordinated with *p*-cymene, and the employment of mixed ligands was quite rare compared to the other homo or hetero aromatics. By now, the application for this brilliant complex has not yet implemented, perhaps due to its comparatively low yields. In addition, Boldyrev further summarised the in silico advances in aromaticity and antiaromaticity for bridging transition-metal clusters by bonding and magnetic analyses [10].

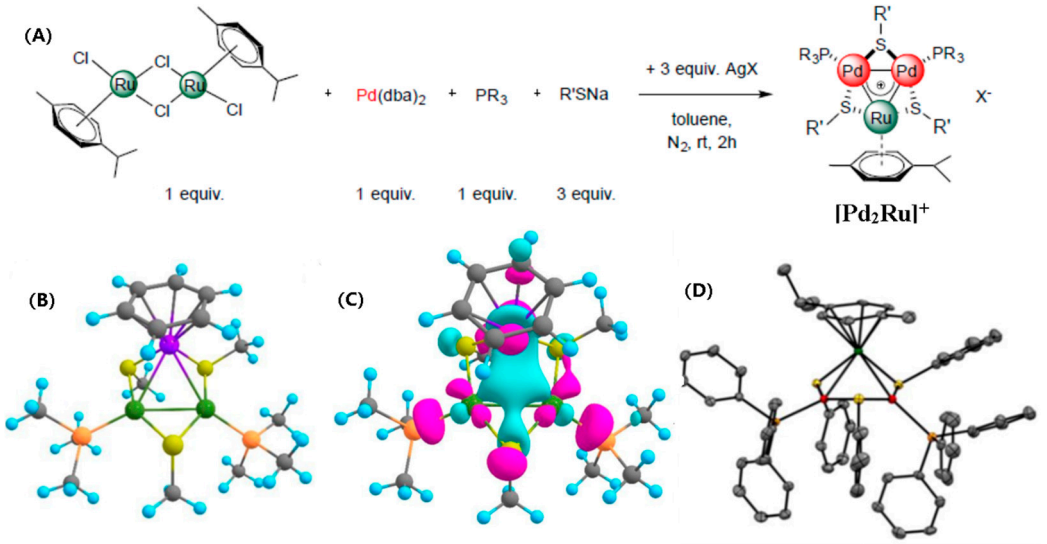

Figure 10. (**A**) Facile synthetic routes for heterobimetallic $[Pd_2Ru]^+$ complexes. (**B**) Simplified model for heteroaromatic $[Pd_2Ru]^+$ complex. Pd-green, Ru-purple, P-orange, S-yellow, C-grey, H-blue. (**C**) The HOMO for the synthesized $[Pd_2Ru]^+$ system. (**D**) Top view for the crystal structure of $[Pd_2Ru]^+$, ellipsoid drawn at 50% probability, Pd (red), Ru (green), P (orange), S (yellow), C (gray). Adapted with permission from ref. [84] Copyright © 2024, Royal Society of Chemistry.

2.8. Triangular σ-Aromatic $[Th_3]^{2-}$

N. Kaltsoyannis and S. T. Liddle synthesized the first σ-aromatic radioactive metal composed tri-thorium cluster $\{Th_3(C_8H_8)_3Cl_6\}^{2-}$, abbreviated as $[Th_3]^{2-}$ (Figure 11) [85,86]. $[Th_3]^{2-}$ was obtained through the interaction of $[K_2\{C_4(SiMe_3)_4\}]$ with $[Th(\eta^8\text{-}C_8H_8)(Cl)_2\text{-}(THF)_2]$. Single-crystal X-ray diffraction showed that $[Th_3]^{2-}$ was equilateral, and the average Th-Th bonds distances (3.99 Å) for the triangle was much lower than the sum of Van der Waals radii for thorium (4.74 Å). Indeed, various DFT and NICS analyses showed that the $[Th_3]^{2-}$ core exhibited a valence-delocalized three-centre-two-electron σ-aromatic character. A short time later, Cuyacot and Foroutan-Nejad made more theoretical comparisons for $[Th_3]^{2-}$, and questioned the employment of the NICS method and opposed the opinion that the Th–Th bond in the $[Th_3]^{2-}$ was aromatic. I believe that further studies of this peculiar triangular $[Th_3]^{2-}$ and the developments for the other predicted triangular metallic aromatics will give a more unified or developed view of triangular all-metal aromaticity.

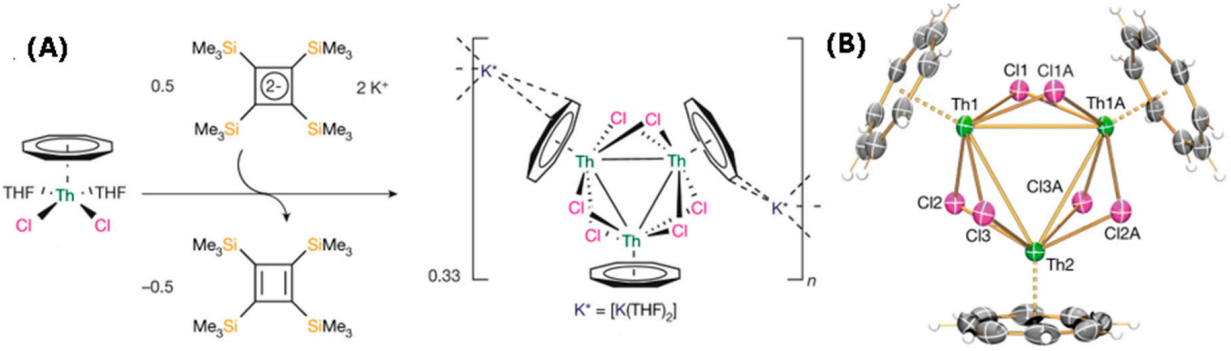

Figure 11. (**A**) Facile synthesis of the tri-Th complex $[\{Th(C_8H_8)(Cl)_2\}_3]^{2-}$ by $[K_2\{C_4(SiMe_3)_4\}]$ and $[Th(\eta^8\text{-}C_8H_8)(Cl)_2(THF)_2]$. (**B**) Crystal structure of $[\{Th(\eta^8\text{-}C_8H_8)(\mu_3\text{-}Cl)_2\}_3\{K(THF)_2\}_2]_\infty$ with 50% probability ellipsoids. Adapted with permission from ref. [85] Copyright © 2024, Springer Nature.

3. Theoretical Predictions of Aromaticity for Triangular All-Metal Clusters

Aside from the above-discussed isolated all-metal aromatics as robust trinuclear crystals or solids, plenty of proposed triangular all-metal structures composed of various transition metals, semimetallics and other metals have been investigated by theoretical calculations in the past decade to predict their potentially possessed all-metal σ, π or δ-aromaticity [87–92]. Some typical and representative examples are discussed in the following for their peculiar structures, predicted triangular all-metal aromaticities and potential powerful applications.

3.1. d-Orbital Aromaticity in Triangular $[M_3O_9]^-$, $[M_3O_9]^{2-}$ (M = W, Mo)

In 2005, Wang and co-workers reported the experimental and theoretical proofs of *d*-orbital aromaticity for early transition metal oxide clusters, $[M_3O_9]^-$ and $[M_3O_9]^{2-}$ (M = W, Mo) [28]. Both theoretical calculations and photoelectron spectroscopy showed that $[W_3O_9]$ and $[Mo_3O_9]$ are aromatic anions and presented D_{3h} symmetric property with a low-lying unoccupied molecular orbital occupied by one or two electrons. The single-occupied molecular orbital (SOMO) for $[W_3O_9]^-$ and the highest occupied molecular orbital (HOMO) for $[W_3O_9]^{2-}$ indicated M–M σ-bonding interactions which were inconsistent with their *d*-orbital aromaticity (Figure 12). The D_{3h} symmetric $[M_3O_9]^{2-}$ dianions were given by adding another electron to this orbital and the three-centre-two-electron (3c–2e) bond was presented.

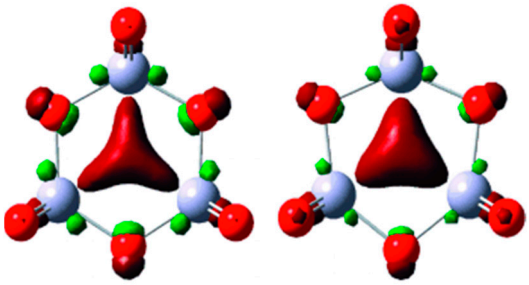

Figure 12. The SOMO for $[W_3O_9]^-$ and the HOMO for $[W_3O_9]^{2-}$. Adapted with permission from ref. [28] Copyright © 2024, Wiley-VCH Verlag GmbH & Co. KGaA, Weinheim, Germany.

According to photoelectron spectroscopy (PES) analysis, the calculated resonance energy (about 1.05 eV) for the $[M_3O_9]^{2-}$ cluster was comparable to the value estimated for highly aromatic benzene. In addition, the NICS values [93] among the ring centre of $[W_3O_9]^{2-}$ and $[Mo_3O_9]^{2-}$ were obtained as −21.5 and −20.5, respectively. So, the $[M_3O_9]^-$ and $[M_3O_9]^{2-}$ clusters described by Wang's group are peculiar with equal M−M bond lengths, large resonance energies and large negative NICS values, which all suggest that they are highly aromatic species involving fully delocalized metal–metal bonds. This new class of *d*-orbital aromatic species exhibited interesting chemical, electrochemical, and catalytic properties even without isolation and full characterization.

3.2. δ-Aromaticity in Triangular $[Ta_3O_3]^-$

Many groups have discovered δ-aromaticity in metallic systems; the presence of δ bonds between identical or different transition-metal atoms indicated that delocalized cyclic δ bonds may exist in cyclic transition-metal structures [94]. However, different from valent *s* or *p* orbitals, *d* orbitals are more sterically restricted. As we know, *d*-orbital aromaticity needs substantial *d*–*d* bonding interactions, so the possibility for the transition metal to participate in forming chemical bonding mainly depends on the type of the transition metals and their spatial coordination circumstances [95–97]. In 2007, Wang and Boldyrev confirmed experimental and theoretical evidence for the presence of δ-aromaticity in the planar D_{3h} symmetric triangular cluster $[Ta_3O_3]^-$ which possessed three

delocalized electrons among Ta–Ta bonding [98]. The authors found the presence of not only π-aromaticity but also *δ*-aromaticity contributed by the *d*-bonding interactions in this proposed $[Ta_3O_3]^-$ cluster according to the photoelectron spectroscopy (PES) [99] analysis under 193 nm (Figure 13a, 6.424 eV) and 157 nm (Figure 13b, 7.866 eV), respectively.

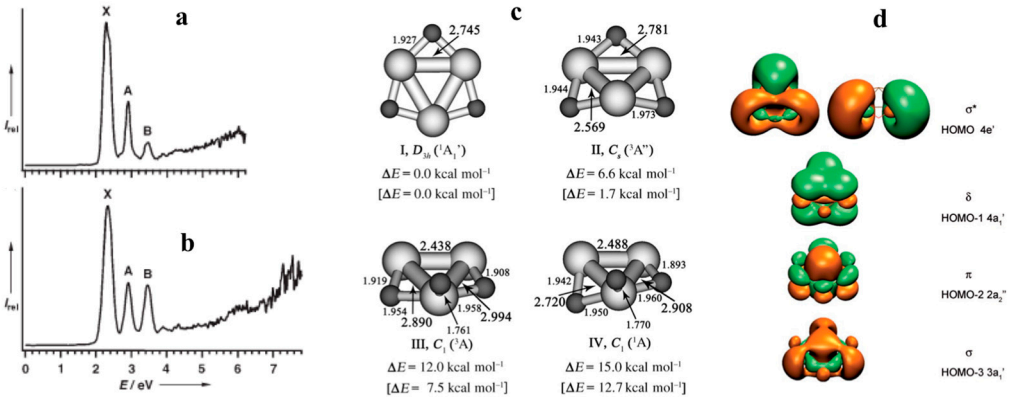

Figure 13. (**a**) Photoelectron spectrum for $[Ta_3O_3]^-$ under193 nm, A, B, X were representative peaks; (**b**) Photoelectron spectrum for $[Ta_3O_3]^-$ under 157 nm. (**c**) Optimized and the representative isomers for the $[Ta_3O_3]^-$. The relative energies Δ*E* and bond lengths for $[Ta_3O_3]^-$. (**d**) The most representative five valence molecular orbitals in the $[Ta_3O_3]^-$. Adapted with permission from ref. [98] Copyright © 2024, Wiley-VCH Verlag GmbH & Co. KGaA, Weinheim, Germany.

In addition, compared with the common ab initio calculations, both the optimized structures and the most representative electronic transition states for $[Ta_3O_3]^-$ indicated that this cluster was arranged in a planar D_{3h} triangle (Figure 13c). Based on the chemical-bonding analysis, the five most representative valence molecular orbitals participated in the Ta–Ta bonding interactions. Concerning the contributions of the 5d atomic orbitals, the close bonding interactions between the *δ* and *π* orbitals of Ta atoms were apparent (Figure 13d). So, the most representative five valence molecular orbitals demonstrated the delocalization of the *δ* bonds and proved that the $[Ta_3O_3]^-$ cluster is another example with *δ*-aromaticity. The ligated $[Ta_3O_3]^-$ cluster has not yet been isolated experimentally.

3.3. d-Orbital Aromaticity in Triangular $[Tc_3X_9]^{2-}$

Decades ago, scientists started the investigations for trinuclear complexes Re_3X_9 (X = Cl, Br, I) and found the electron delocalization character for these potential three-membered metallic cores [30,32,33]. However, the technetium analogues (Figure 14) gained less attention until Weck and coworkers reported their study for the technetium halide complexes $[Tc_3(\mu\text{-}X)_3X_6]^{0/1-/2-}$ (X = F, Cl, Br, I), which were further confirmed as isomorphous with their rhenium congeners by density functional theory calculations [88]. Even without isolation, the theoretical calculation results via adaptive natural density partitioning demonstrated that the $[Tc_3X_9]^{2-}$ complex could exhibit aromaticity contributed by the *d*-orbital-based *π* electron delocalization over the tri-technetium centre.

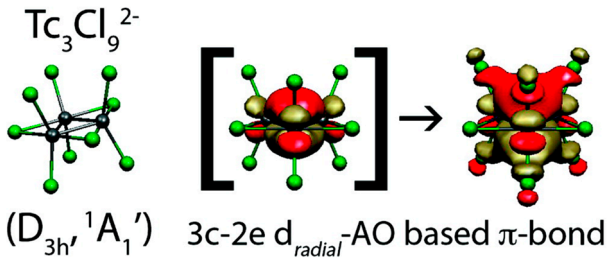

Figure 14. The *d*-orbital-based DFT calculation for trinuclear aromatic $[Tc_3Cl_9]^{2-}$. Reprinted with permission from ref. [88] Copyright 2011, American Chemical Society.

3.4. Aromaticity/Antiaromaticity of Triangular $[Sc_3]^-$

Rashidi-Ranjbar, Ruud, Foroutan-Nejad and coworkers reported new insights on the determination of aromaticity in triangular all-metal clusters $[Sc_3]^-$ by giving computational arguments with the help of the ring-current model over local indices [100]. With their efforts, the evidence of the magnetic aromaticity was confirmed by nucleus-independent chemical shifts. Two typical methods for estimating magnetically induced ring currents were employed; the first approach was based on the quantum theory of atoms in molecules (QTAIM) and the second approach was explicit calculation using the magnetically induced current densities. Using the QTAIM-based magnetizabilities principle, they explained the presence of the two-zone aromaticity/antiaromaticity of several 3d all-metallic triangular clusters including Sc_3^-, Cu_3^+ and Cu_4^{2-} (Figure 15). According to the classical electromagnetic theory, their theoretical investigations indicated a comprehensive explanation for the anomalous magnetic shielding in different transition metal cluster. The authors also appealed that the nature of magnetic aromaticity/antiaromaticity for all types of triangular transitional all-metal complexes should be determined more comprehensively based on more reliable global indices.

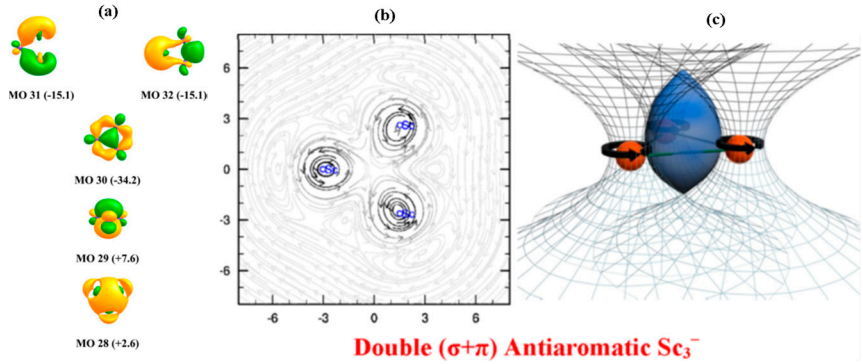

Figure 15. (**a**) Representative molecular orbitals of anionic $[Sc_3]^-$ and their contributions to NICS(0)MO_{zz}. (**b**,**c**) The two-zone aromaticity/antiaromaticity character for metallic $[Sc_3]^-$ via the QTAIM-based magnetizabilities. Reprinted with permission from ref. [100] Copyright 2013, American Chemical Society.

3.5. Aromaticity of Triangular $[Al_3]^-$

With strong interest, a multiconfigurational high-level electronic structure calculation method was employed to investigate the aromaticity property for the triangular all-metal cluster $[Al_3]^-$ by Ugalde's group (Figure 16a). Explicit theoretical calculation values indicated that the proposed three-membered-ring-like cluster anion Al_3^- presented the three most representative close low-lying electronic states with clearly different spins, and all these states presented strong multiconfigurational properties. Ugalde and coworkers further studied the aromaticity character of the all-metallic cluster $[Al_3]^-$ using the total electron delocalization method. The related evaluations of the normalized multicentre electron delocalization indices for each state were calculated according to the multiconfigurational wave functions [101]. Combining the multifaceted results, the authors concluded that the lowest-lying singlet and triplet states of Al_3^- were proved to be highly aromatic. In contrast, the closest lowest-lying state (the quintet state) presented much fewer aromatic properties (Figure 16b). Later, theoretical investigations for the d-p hybridized aromaticity, neutral salts and photoelectron spectroscopy of the proposed LaX_2^- (X = Al, Ga, In) clusters were calculated [102]. Near-degenerate molecular-orbital-coupling-induced dual aromaticity in stable open-shell metal clusters was also observed [58]. Furthermore, the possibilities and behaviors of the aluminium trimer during the combination with different superatom clusters were illustrated [103].

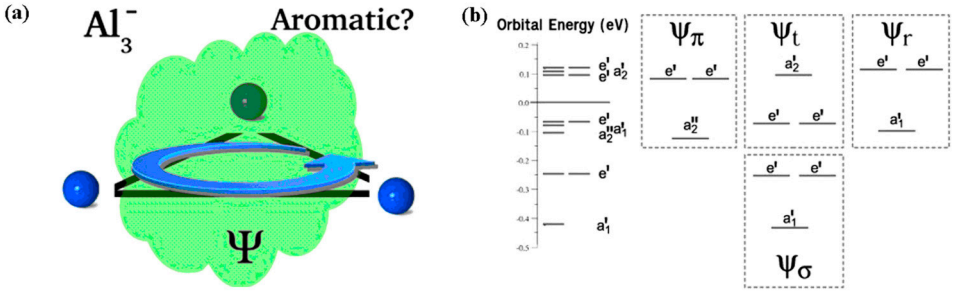

Figure 16. (**a**) The most representative and highly aromatic lowest-lying singlet and triplet states of the all-metal-ring-like cluster Al_3^-. (**b**) Valence molecular orbitals of D_{3h} symmetric cluster Al_3^- arranged in increasing energy and grouped into four independent aromatic systems, Ψ_σ, Ψ_r, Ψ_t, and Ψ_π. Adapted with permission from ref. [101] Copyright © 2024, Wiley-VCH Verlag GmbH & Co. KGaA, Weinheim, Germany.

3.6. Aromatic in Triangular $[M_3]^{4+}$ (M = Ni, Pd, Pt)

Xiao and Li reported the structural, electronic and bonding properties of a system of triangular trinuclear clusters $[M_3X_3]^+$ (M = Ni, Pd, Pt; X = F, Cl, Br, I) and explored the electronic and steric effects on the adsorptions of H_2 and other small molecules (Figure 17A) [104]. The authors presented the chemical bonding models of M_3 in detail and proposed that the oxidation state of each metal element in the M_3 cluster was +4/3. In fact, combined with the experimental successes on the isolations of $[M_3]^+$ (M = Pd, Pt) crystals by Malacria's group, all-metallic σ-aromaticity was also confirmed in these triangular all-metal clusters by theoretical calculations. It was suggested that by changing the energies and compositions of M–M and M–L chemical bonding orbitals, the stability and the catalytic activity of these complexes could be adjusted. The orbital interactions and relativistic effects could be responsible for the active H_2 dissociative adsorption on these complexes. This finding offered another example of adjusting catalytic properties by tuning different chemical bonding in the all-metal clusters. Actually, similar conclusions have been confirmed experimentally by the highly efficient triangular all-metal aromatic cluster $[Pd_3]^+$-catalyzed internal alkyne reduction reactions. Later, the effects of ligands on bonding stability and σ-aromaticity for Pt nanoclusters were also examined [105]. Modulation of the backside-ligand effect of main-group aromatic ligands (benzene or naphthalene) binding to Pd was also investigated [106].

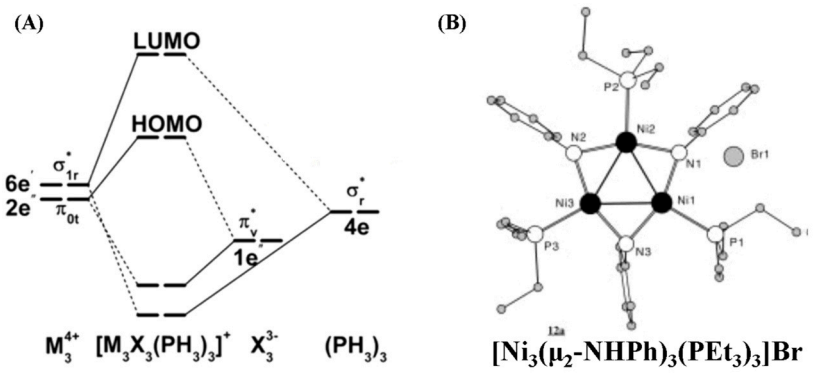

Figure 17. (**A**) The bonding properties of trinuclear clusters $[M_3X_3]^+$ (M = Ni, Pd, Pt; X = F, Cl, Br, I). Reprinted with permission from ref. [104] Copyright 2017, American Chemical Society. (**B**) Crystal structure for the C_3 symmetric triangular tri-nickel cluster $[Ni_3(PEt_3)_3(\mu_2\text{-}NHPh)_2]Br$. Reprinted with permission from ref. [107] Copyright © 2024 WILEY-VCH Verlag GmbH & Co. KGaA, 69451 Weinheim, Germany.

According to the earlier report of Fenske, treating transition metallic complex $NiBr_2(PEt_3)_2$ with Li_2NPh in THF/*n*-Heptane gave nitrogen-bridged triangular tri-nickel

cationic cluster $[Ni_3(\mu_2\text{-}NHPh)_3(PEt_3)_2]Br$, abbreviated as $[Ni_3]^+$ [107]. This $[Ni_3]^+$ cluster was investigated using single-crystal X-ray diffraction (Figure 17B). The crystallographic data proved that $[Ni_3]^+$ was C_3 symmetric and composed of a Ni_3-ring with Ni–Ni bond distances ranging from 247.9(1) to 250.6(1) pm, which were the shortest as known and connected with three μ_2-bridging phenylamido ligands. Besides that, similar to their Pd/Pt analogues, each Ni atom was coordinated with one PEt_3 ligand. All Ni atoms lay in a plane, resulting in a trigonal-planar structure. Even the authors claimed that this $[Ni_3]^+$ cluster was closer to the non-aromatic palladium compound discussed by Lee and Trogler [108]. However, according to the comprehensive investigations for their Pd/Pt analogues, all geometric parameters for $[Ni_3]^+$ cluster hinted at the possibility of aromaticity in the triangular all-metal core. Taken together with the theoretical calculations, the triangular tri-nickel cationic cluster $[Ni_3]^+$ may be another close analogue to the aromatic systems $[Pd_3]^+$ and $[Pt_3]^+$, which are isolobal to π-aromatic $[C_3H_3]^+$, whereas further explicit theoretical calculations would be required to give a definitive conclusion on its proposed all-metal π-aromaticity.

3.7. Triangular Aromatic Heterobimetallic $[Hf_3]^+$

Boldyrev presented that the lowest singlet $D_{3h}{}^1A_1$ structure of $[Hf_3]^+$ is another example of a triple (σ-, π-, and δ-) aromatic system (Figure 18) [109]. An extensive search for the structure of Hf_3 using the B3LYP/LANL2DZ theory revealed that the lowest triplet and singlet states are $D_{3h}{}^3A_2'$ and $D_{3h}{}^1A_1'$, respectively. Notably, the triplet state for $[Hf_3]^+$ was the lowest one. However, the authors discovered that these two states are degenerate at the CASSCF/Stuttgart+2f1g level. These results indicated that the singlet state could be the global minimum structure at the higher level of theory. They concluded that the triplet $D_{3h}{}^3A_2'$ structure was doubly (σ- and π-) aromatic and the singlet $D_{3h}{}^1A_1'$ structure was the first reported triple (σ-, π-, and δ-) aromatic system.

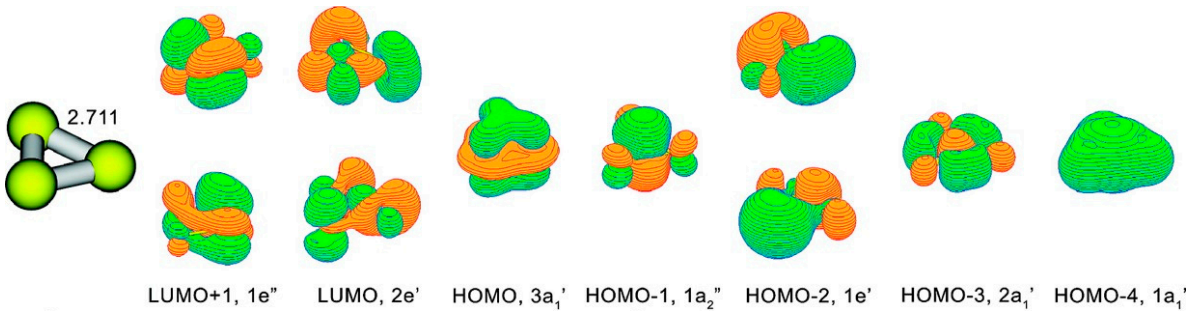

Figure 18. Triple (σ-, π-, and δ-) aromaticity for the Hf_3 cluster in the Lowest D_{3h}, $^1A_1'$ state. Reprinted with permission from ref. [109] Copyright © 2024, American Chemical Society.

3.8. Triangular Aromatic $Os_3N_3^{+/-}$

Jin's group investigated the stability, electronic character, and aromaticity of osmium-nitride clusters $Os_3N_3^{+/-}$ using DFT (B3LYP methods) (Figure 19) [110]. The theoretical calculations revealed that five types of interactions existed in the hexagonal $Os_3N_3^+$ (D_{3h}, $^7A_1'$) cation and the regular planar $Os_3N_3^-$ (D_{3h}, $^5A_1'$) anion. Through detailed molecular orbitals (MOs) analysis, the authors concluded that the cationic $Os_3N_3^+$ (D_{3h}, $^7A_1'$) and anionic $Os_3N_3^-$ (D_{3h}, $^5A_1'$) possessed a triple-aromatic character (σ-, π- and δ-aromaticity), simultaneously. It was convinced that the solid structural stability was contributed by the five types of powerful *d*-orbital bonding interactions and triple aromaticity. Based on the aromaticity of the bare osmium trimers, the authors further calculated their binding interactions to group IA/IIA of all-metal series [111].

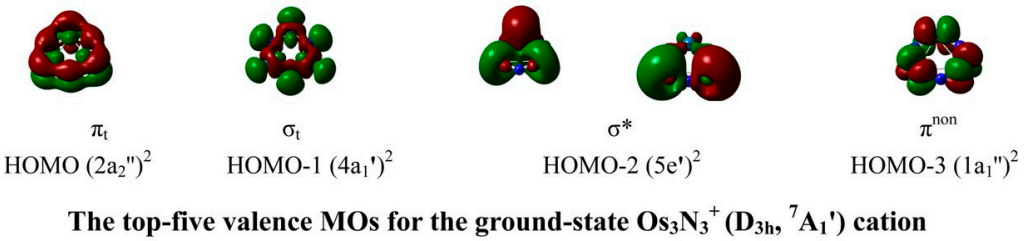

Figure 19. Theoretical calculations for the σ-, π-, and δ- aromaticity in the $Os_3N_3^{+/-}$ clusters. Reprinted with permission from ref. [110] Copyright © 2024 Elsevier BV.

3.9. Aromaticity in Triangular $Ir_3N_3^{+/-}$

In 2017, Ding and coworkers fully investigated the chemical bonding, aromaticity and stabilities of the ground state of iridium low-nitride $Ir_3N_3^{2+/0/2-}$ clusters (Figure 20), their metal complexes $Ir_3N_3M^{-/0}$ (M = Li, Na, K and Be, Mg, Ca) and bimetallic complexes $Ir_3N_3M_2$ (M = Li, Na, and K) using DFT calculations [112]. Through detailed molecular orbitals (MOs) analysis, they reveal that the neutral Ir_3N_3 (D_{3h}, $^3A_2''$) cluster possesses σ-, π-, and partial δ- aromaticity, and the $Ir_3N_3^{2-}$ (D_{3h}, $^1A_1'$) dianion possesses both σ- and π-aromaticity. They further proved that the pyramidal $Ir_3N_3M^{-/0}$ and bipyramidal $Ir_3N_3M_2$ complexes also possess aromatic characters and preserved the $Ir_3N_3^{2-}$ (D_{3h}, $^1A_1'$) motif.

Figure 20. The top-two representative valence MOs for ground state $Ir_3N_3^{2-}$ (D_{3h}, $^1A_1'$) motif. Reprinted with permission from ref. [112] Copyright © 2024 Elsevier BV.

3.10. Aromaticity in Triangular PrB_2^-

Due to their highly contracted 4f atomic orbitals, lanthanide metals were rarely found in multiple types of aromatic systems. The first example was the lanthanide-boron PrB_2^-, which was confirmed as a double-aromatic triatomic molecule based on joint investigations in photoelectron spectroscopy and quantum calculations (Figure 21) [113]. Global minimum structural studies revealed that PrB_2^- possessed a C_{2v} triangular structure. Their paramagnetic triplet $^3B_2$ electronic ground state could be viewed as featuring a B_2^{4-} and one trivalent Pr(III, f^2). Chemical bonding analyses concluded that cyclo-PrB_2^- showed multiple Pr–B bonding characters and exhibited σ and π double aromaticity. This smallest 4f-metalla-aromatic system PrB_2^- also highlighted the formation of the rare B_2^{4-} tetra-anion, completing the isoelectronic C_2^{2-}, N_2, and O_2^{2+} series.

According to the Geerlings findings, the metal–metal bonding interactions were much more complicated in the $[Li_3]^+$ system [114]. Using the ring-current map computation, the assumed σ-aromaticity for the triangular $[H_3]^+$ and $[Li_3]^+$ was investigated. The $[H_3]^+$ showed a characteristic diatropic ring current and could be considered as σ-aromatic on the magnetic criterion. However, even with a negative NICS value, $[Li_3]^+$ was concluded to be non-aromatic according to the same criterion because it did not show any global current.

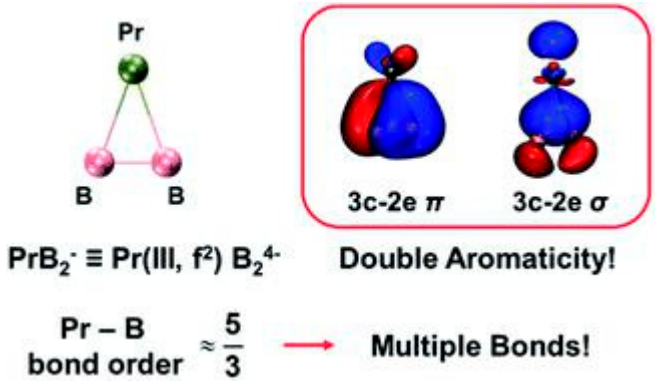

Figure 21. The smallest 4f-metalla-aromatic molecule of cyclo-PrB_2^- with Pr-B multiple bonds. Adapted with permission from ref. [113] Copyright © 2024, Royal Society of Chemistry.

4. Catalytic Applications of Triangular All-Metal Aromatic Clusters

For trimetallic systems, scientists are becoming more and more interested in the investigations of their applications and synergistic effects. Clearly, triangular all-metal aromatic clusters contained characteristic delocalized cyclic electrons, metal–metal bonding interactions which determined their good stabilities, and aromaticity, making them become the metallic counterparts of the main-group aromatics. Different from biased opinions on all-metal aromatics for weak stability and rare utilizations, triangular all-metal aromatics were found to show great potential in applications like catalysis, coordination, and material science. In the following part, the most representative examples were summarized.

4.1. σ-Aromatic Tri-Gold Cation $[Au_3]^+$ Catalyzed Amine Carbonylation

The first example referring to the applications of all-metal aromatics in catalytic reactions was reported by Bertrand and coworkers. They presented the syntheses and stabilities for the NHC stabilized aromatic tri-gold complex $[Au_3]^+$ (Figure 22B), and further investigated their catalytic behaviors and plausible mechanisms in the carbonylation reaction [66,67]. Several types of transition metal catalysts presented efficiencies for the reaction of primary amines and carbon monoxide to prepare urea derivatives [115–117]. The tri-gold cluster was employed to catalyze this reaction and proved to be a green and selective catalyst (Figure 22A). The triangular all-metal aromatic $[Au_3]^+$ catalyzed carbonylation reaction offered various corresponding substituted urea with mild yields. In order to achieve higher conversions, the catalyst loading reached 2.5 mol% in this reaction. Notably, the isolated yield for the corresponding substituted urea was much lower when the use of the catalyst was decreased. In addition, the substrate scope of this catalytic carbonylation reaction was screened and it was found that fewer spatially hindered amines could be transformed into urea derivatives with higher yields. The authors claimed a peculiar reaction mechanism for this aromatic tri-gold complex $[Au_3]^+$ catalyzed carbonylation of amines. This proposed mechanism involved an oxidation of the valence state of the gold from $Au_2^0Au^I$ to Au_3^I, whereas this proposal demonstrated that these $[Au_3]^+$ clusters lost their aromatic nature as an intermediate. Meanwhile, the more plausible catalytic mechanism is still underway. This reaction also had previously been screened by using the other types of gold-containing catalysts like mono-gold complexes and gold nanoparticles [118,119]. Generally, simple gold complexes presented good activity in this model reaction; for example, Corma et al. showed that small metallic gold clusters could display higher catalytic activities even than small-sized gold nanoparticles and many mono-gold catalysts [120–123]. Later, the behaviors of σ-aromatic cyclic $[M_3]^+$ (M = Cu, Ag, Au) complexes were investigated when dimethyl imidazol-2-ylidene, isoxazole, pyridine, furan, carbon monoxide and noble gases were introduced for complexation [124]. In addition, the cyclic $(R_2SnAu)_3$ anion was proposed to be stable and showed in-plane σ-Möbius aromaticity [125].

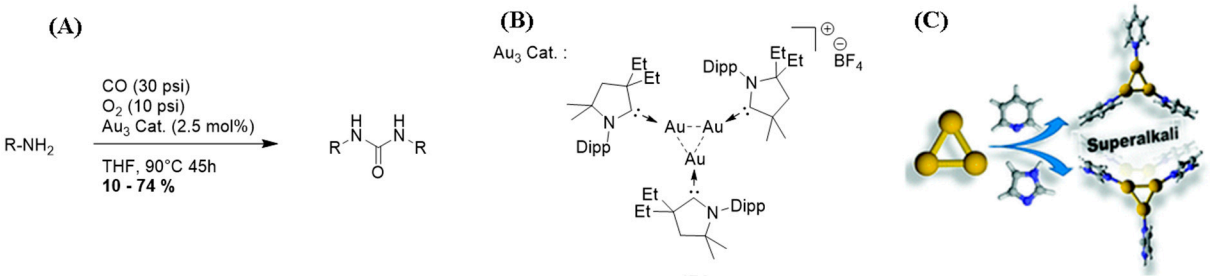

Figure 22. (**A**) Aromatic tri-gold $[Au_3]^+$ catalyzed amine carbonylation in the presence of oxygen. (**B**) Structure of aromatic trigold catalyst $[Au_3]^+$ with substituted NHC as ligand. Adapted with permission from ref. [67] Copyright © 2024, Wiley-VCH Verlag GmbH & Co. KGaA, Weinheim, Germany. (**C**) Proposed superalkali complex made of an all-metal aromatic trigonal Au_3 core and pyridine (Py) or imidazole (IMD) ligands. Adapted with permission from ref. [126] Copyright © 2024, Royal Society of Chemistry.

Compared to the usual alkali and alkaline earth metals, analogues super alkalis showed lower ionization energy and possessed peculiar properties. According to the First Principles calculations, predicted superalkali clusters containing triangular all-metal aromatic Au_3 coordinated with either three imidazole (IMD) or three pyridine (Py) ligands are very possibly to be stable (Figure 22C) [126]. Similar to the properties of superalkali clusters, the calculated ionization energies (IE) for the organometallic complexes, $Au_3(Py)_3$ or $Au_3(IMD)_3$, are quite low. Additionally, the first-order hyperpolarizability calculations proved that some of these coordinated complexes presented non-linear optical properties, which were also similar to the properties of normal super alkali.

Based on the above work on gold clusters, our group synthesized the first triphenylphosphine stabilized triangular tri-gold complex $[(PPh_3Au)_3]^+BF_4^-$ through the facile reduction of μ^3-oxo complex $[\mu_3\text{-}O(PPh_3Au)_3]^+BF_4^-$ (Figure 23) [127]. The cyclic voltammetry of $[(PPh_3Au)_3]^+BF_4^-$ showed one single oxidation process. These tri-gold complexes were further employed in the catalytic hydroamination of phenylacetylenes with anilines. When the loading was decreased to 1.0 mol%, 95% of conversions were obtained. When the catalyst loading further decreased to 0.5 mol%, 83% of isolated yields were achieved in the preparative scale. This application presented great significance in the synthesis of imine-containing pharmaceutical intermediates. Moreover, further investigations of the catalytic mechanisms indicated that these tri-gold complexes played roles as pre-catalysts in the hydroamination.

4.2. Aromatic $[Pd_3]^+$ Catalyzed Semi-Reduction of Internal Alkynes

Trinuclear all-metal aromatic $[Pd_3]^+$ should be a good choice for catalytic applications in many types of reactions due to their essential palladium-containing nature and delocalized metal–metal bonding forms. In order to investigate the catalytic properties of all-metal aromaticity in $[Pd_3]^+$, Malacria's group investigated the catalytic properties of these tripalladium complexes in the classical semihydrogenation reaction of internal alkynes which were used as a model reaction for many types of mono-palladium complexes [128–132]. They found that when palladium clusters $[Pd_3]^+$ were employed to reduce internal alkynes in a hydrogen transfer condition, quantitative (Z)-alkenes were obtained without forming any trace of alkane products [133]. The activity and selectivity for these $[Pd_3]^+$ clusters are comparable with the best mono-palladium peers. At the end of the reaction, the HRMS still detected a trace of the complement catalyst.

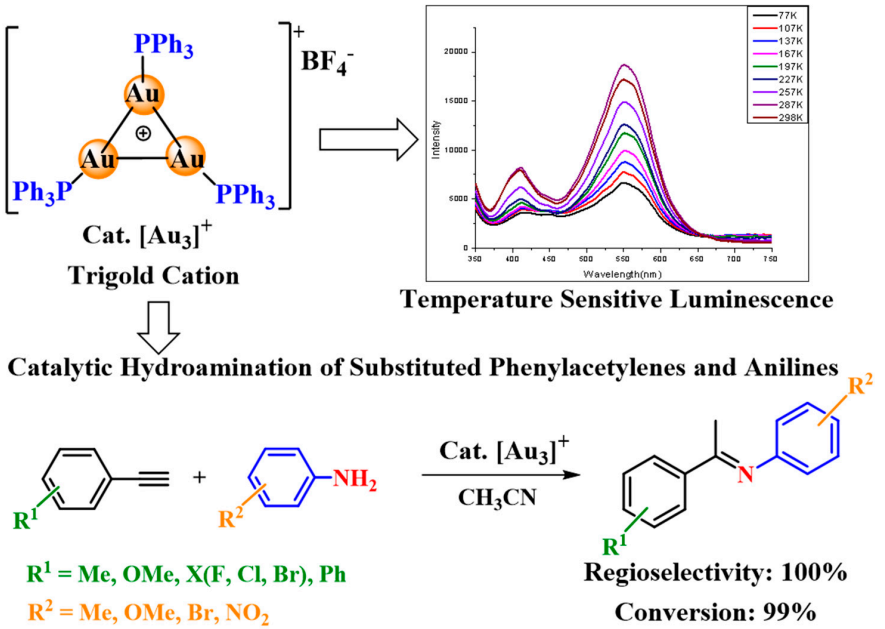

Figure 23. Triphenylphosphines stabilized triangular gold clusters and their application in hydroamination. Reprinted with permission from ref. [127] Copyright © 2024 WILEY-VCH Verlag GmbH & Co. KGaA, 69451 Weinheim, Germany.

In contrast to the excellent catalytic behavior of the $[Pd_3]^+$ complex, the aromatic triangular tri-platinum complex $[Pt_3]^+$ showed inert behavior under identical conditions. In order to explain their vastly different catalytic behaviors, the most representative frontier molecular orbitals of the analogues structures $[Pd_3]^+$ and $[Pt_3]^+$ were compared and analyzed (Figure 24A). The LUMO of the active $[Pd_3]^+$ triangle is obviously lower than that of the heavier $[Pt_3]^+$ cluster with the ΔE_{gap} reached to 14.9 kcalmol^{-1}. On the contrary, according to the literature research on palladium cluster-catalyzed reactions [134–136], monoatomic π-acidic Pd-containing clusters are much less electrophilic than their Pt-containing analogues.

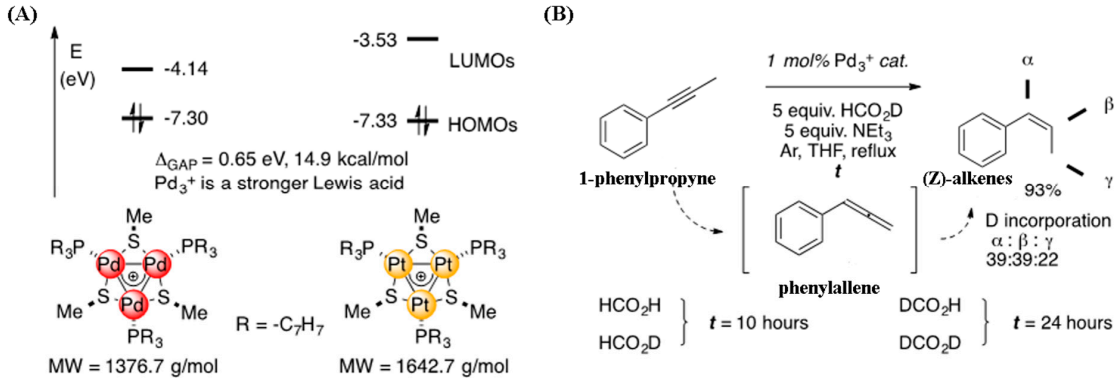

Figure 24. (**A**) Energies of the most representative frontier molecular orbitals of $[Pd_3]^+$ and $[Pt_3]^+$ complexes, values in eV. (**B**) Deuterium-labelling experiment process. Adapted with permission from ref. [133] Copyright © 2024, Wiley-VCH Verlag GmbH & Co. KGaA, Weinheim, Germany.

The authors also carried out the deuterium-labelling experiment to figure out the possible catalytic pathways (Figure 24B). They found that deuterium atoms incorporated on the terminal carbon of 1-phenylpropyne with $[Pd_3]^+$ complex as the catalyst and the intermediate phenylallene was formed during the catalytic reaction [137]. These findings indicated that the hydrogen transfer step might be rate-determining. In addition, the kinetic studies presented that the hydride-transfer process displayed obvious isotopic effects [138].

Later on, Malacria's group further discovered that the semi-hydrogenation of internal alkynes could also be catalyzed by the aromatic $[Pd_3]^+$ clusters under neat conditions and gave *cis*-alkenes with quantitative conversions (Figure 25A) [139]. The authors claimed that when 0.03 mol% amount of catalyst was loaded, a large gram scale of the catalytic semi-hydrogenation could be carried out successfully. This group further developed the zwitterionic $[Pd_3]^+$ clusters and employed them in the semi-reduction reaction of internal alkynes as pre-catalysts or as a whole complex. These catalysts propelled the reaction which could be carried out under even neat conditions (Figure 25B) [140]. Generally, triangular all-metal aromatic $[Pd_3]^+$ complexes presented excellent catalytic activities and outstanding selectivity in the semi-reduction of internal alkynes mainly due to their intrinsic aromaticity-induced stability. Aromatic tripalladium complexes could also catalyze inter/intramolecular cascade reactions of 1,6-enynes and carboxylic acids, giving excellent catalytic activities and selectivities [141].

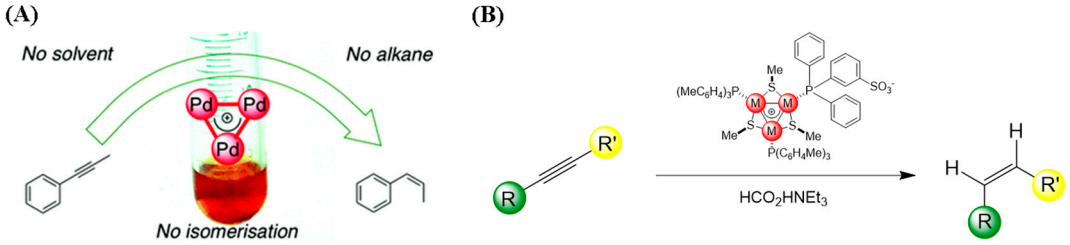

Figure 25. (**A**) Aromatic $[Pd_3]^+$ complexes catalyzed hydrogen transfer reactions of internal alkynes and showed quantitative *cis*-selectivity. Adapted with permission from ref. [139] Copyright © 2024, Royal Society of Chemistry. (**B**) Zwitterionic aromatic $[Pd_3]^+$ complexes catalyzed semi-reduction reaction of internal alkynes. Adapted with permission from ref. [140] Copyright © 2024, American Chemical Society.

Through a regular ion exchange process, anionic MOFs could become frameworks or templates with interesting properties. For example, crystalline MOFs could be further functionalized due to their modular character and novel properties could occur after elaborations. Ma and coworkers presented that by a simple ion exchange process, the trinuclear palladium complex $[Pd_3]^+$ could be introduced to the anionic metal–organic framework (MOFs). In addition, the combined catalytic system was heterogeneous and showed excellent catalytic activity in the classical semi-reduction reaction of internal alkynes (Figure 26) [142]. The authors claimed that the thiol groups from the tri-palladium cluster and the delicate pore sizes of the MOF material significantly minimized the aggregations of palladium clusters during the recyclable catalytic process.

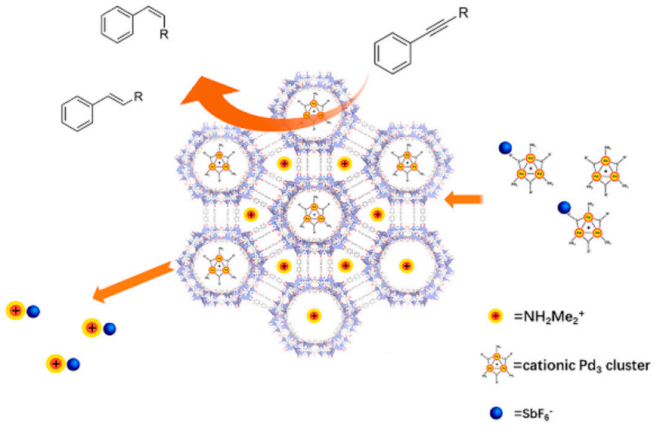

Figure 26. Triangular palladium cations $[Pd_3]^+$ incorporated metal–organic framework and their excellent reactivity in the semi-reduction of internal alkynes. Adapted with permission from ref. [142] Copyright © 2024, American Chemical Society.

4.3. Aromatic $[Pd_3]^+$ Catalyzed Cycloisomerization of 1,6-Enynes and Dienynes

Besides the semi-reduction reaction of internal alkynes, the triangular all-metal aromatic $[Pd_3]^+$ complexes were further applied in the cycloisomerization reactions of substituted internal dienynes and terminal 1,6-enynes and also presented excellent catalytic activity and great selectivity under mild conditions (Figure 27A) [143]. The authors prepared various polycyclic frameworks by modification of substrates and assumed the mechanism of the reaction as a complex cascade process. T Interestingly, the authors later found that the substituted 1,6-enynes showed much different reactive properties when the reaction used carboxylic acid as an additive in the presence of an identical catalyst (Figure 27B) [144]. The catalytic activities of $[Pd_3]^+$ complexes in this cyclisation reaction were comparable to that of much-reported mononuclear Pd(I) and Pd(II) clusters [145,146]. Different from the inertness in the semi-reduction reaction, the analogues tri-platinum catalyst $[Pt_3]^+$ showed good reactivity to cyclize the substrate. However, the authors found that when the analogues tri-palladium complex $[Pd_3]^+$ was used under identical conditions, successive cyclization/double bond shifts happened. So, the tri-platinum catalyst $[Pt_3]^+$ showed a completely different reactive orientation compared with the analogues tri-palladium complex $[Pd_3]^+$ mainly due to their different metallic properties.

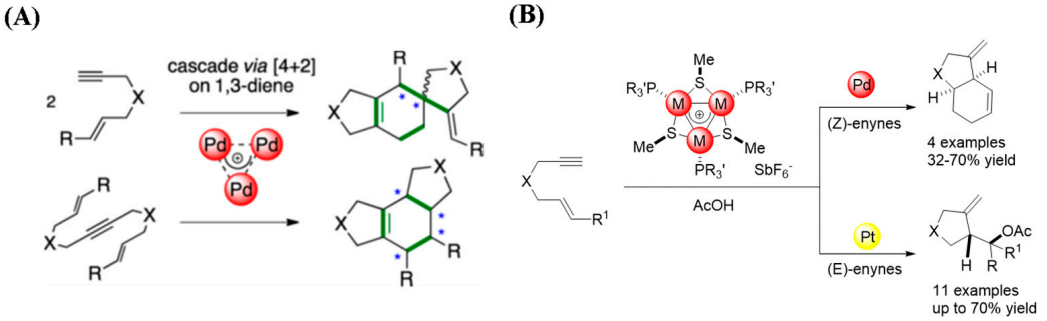

Figure 27. (**A**) Syntheses of functionalized tricyclic cyclohexenes from terminal 1,6-enynes and internal dienynes through aromatic tripalladium complex $[Pd_3]^+$ catalyzed cycloisomerization reaction. Adapted with permission from ref. [143] Copyright © 2024, American Chemical Society. (**B**) Aromatic tripalladium complex $[Pd_3]^+$ catalyzed cycloisomerization of 1,6-enynes in the presence of carboxylic acid. Adapted with permission from ref. [144] Copyright © 2024, Georg Thieme Verlag Stuttgart.

4.4. Aromatic $[Pd_3]^+$ Catalyzed Coupling Reactions

Besides the above applications in semi-reduction of internal alkynes and cyclisation, $[Pd_3]^+$ also has been successfully applied to various types of carbon–carbon coupling reactions by several groups. Zhu and coworkers reported another type of tri-palladium complex $[Pd_3Cl(PPh_2)_2(PPh_3)_3]^+[SbF_6]^-$, abbreviated as Pd_3Cl, which was not C_3 symmetry and stabilized by one chlorine atom and two types of aryl phosphine ligands (Figure 28A) [147]. Compared with the other palladium-complex-catalyzed coupling reaction process [148,149], Pd_3 clusters presented precious C–X (X = halogens) selectivity and excellent efficiency. Pd_3Cl was proved to be a robust and air-stable cluster during characterization and application. The authors pointed out the σ-aromaticity for the Pd_3Cl cluster and also claimed that their outstanding stability was mainly contributed by their delocalized 3c–2e Pd–Pd–Pd bonds among the tri-palladium core. One of the most persuasive proofs for the existence of σ-aromaticity was the presence of delocalized 3c–2e σ-bonds.

Later, Pd_3Cl was further used in homogeneous catalysis with the Suzuki–Miyaura coupling as the model reaction under mild conditions. Among palladium complexes or nanoparticle-catalyzed aryl–aryl bond formation reactions, the Suzuki–Miyaura coupling is one of the most powerful pathways to construct versatile unsymmetrical. The authors investigated the catalytic mechanism of the reaction by monitoring the reaction of simple aryl bromides and arylboronic acids using HRMS and confirmed the presence of possible intermediates in the catalytic circle (Figure 28B). Interestingly, they found the mass for the Ar inserted intermediate through the simple substitution of the Cl atom between

two palladium atoms and gave a new understanding of the palladium clusters involved mechanisms of C–C cross-coupling. Additionally, besides aryl bromides, the authors omitted the cases of the aryl chlorides and aryl iodides in this work and did not figure out the halogen selectivity in this case. Even though the mass of the Arinserted intermediate was detected, the proposed catalytic circle was not compliant with the widely recognized palladium-catalyzed coupling reactions.

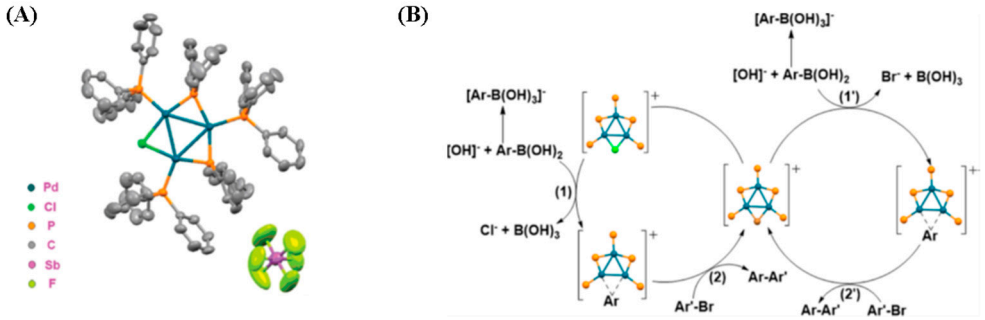

Figure 28. (**A**) The crystal structure of $[Pd_3Cl(PPh_2)_2(PPh_3)_3]^+[SbF_6]^-$. (**B**) Proposed reaction mechanism for the Suzuki reaction catalyzed by $[Pd_3Cl(PPh_2)_2(PPh_3)_3]^+[SbF_6]^-$. Reprinted with permission from ref. [147] Copyright 2017, American Chemical Society.

Later, Schoenebeck and coworkers presented another robust palladium trimer using a facile synthetic method [150]. This palladium triangle possessed C_3 symmetric property and was stabilized by only one type of phosphine ligand. Different from the Pd_3Cl analogue, the Schoenebeck $[Pd_3]^+$ presented unambiguous reactivities and privileged capabilities to C–I bond over C–Br and C–Cl bonds in aryl–aryl bond formations from polyhalogenated arenes and Grignard reagents (Figure 29). The catalytic procedure was classical, using the preformed palladium trimer allowed for quantitative preparation for the arylations and alkylations even for the coupling of steric substrates. Experimental data combined with computational investigations presented the feasibility and capability of the palladium trimer. Even the authors did not mention it, we believe this palladium core $[Pd_3]^+$ presented unique C–I selectivity due to its aromaticity and stability. The cross-coupling catalyst $Pd(OAc)_2/2PPh_3$ could form a dinuclear Pd^I complex and further cyclic Pd_3 clusters during the catalytic process [151].

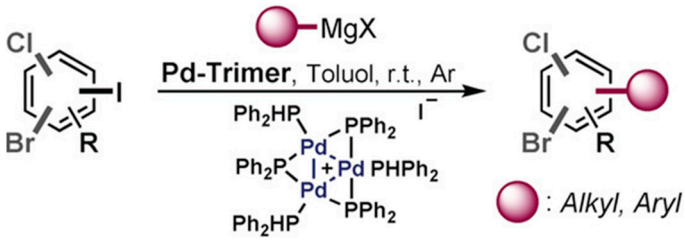

Figure 29. C–I-selective cross-coupling catalyzed by a C_3 symmetric cationic palladium trimer. Adapted with permission from ref. [150] Copyright © 2024, Wiley-VCH Verlag GmbH & Co. KGaA, Weinheim, Germany.

Most importantly, another aromatic tri-palladium complex $[Pd_3]^+$ which was simultaneously stabilized by the sulfur and triaryl phosphine ligands showed outstanding photoelectric properties and was subsequently employed in the Suzuki–Miyaura coupling reaction by our group (Figure 30A) [152]. These C_3-symmetric triangular palladium complexes $[Pd_3]^+$ showed great catalytic activity and exclusive C–X selectivity to aryl iodine thanks to the stability of the catalyst and the mild dissociation energy of the C–I bond. The substrate scope could be extended to thiophene, pyridine, pyrazine, and other common heterocyclic aromatic hydrocarbons. Research on the catalytic mechanism demonstrated that the reaction may involve the intermediate that one sulfur ligand was substituted by

the iodine atom monitored by HRMS. A small amount of this tri-palladium complex $[Pd_3]^+$ (0.06 mol%) showed powerful catalytic activity in the gram scale reaction and gave a 93% yield. For the Sonogashira and Heck coupling reactions, this triangular palladium complex $[Pd_3]^+$ also presented unique selectivity for C–I bonds over the other halogen analogues (Figure 30B) [153]. HRMS monitoring for these two coupling reactions showed that the robust $[Pd_3]^+$ remained as a whole at the end of the catalytic process, which proved that the $[Pd_3]^+$ complex was extremely stable.

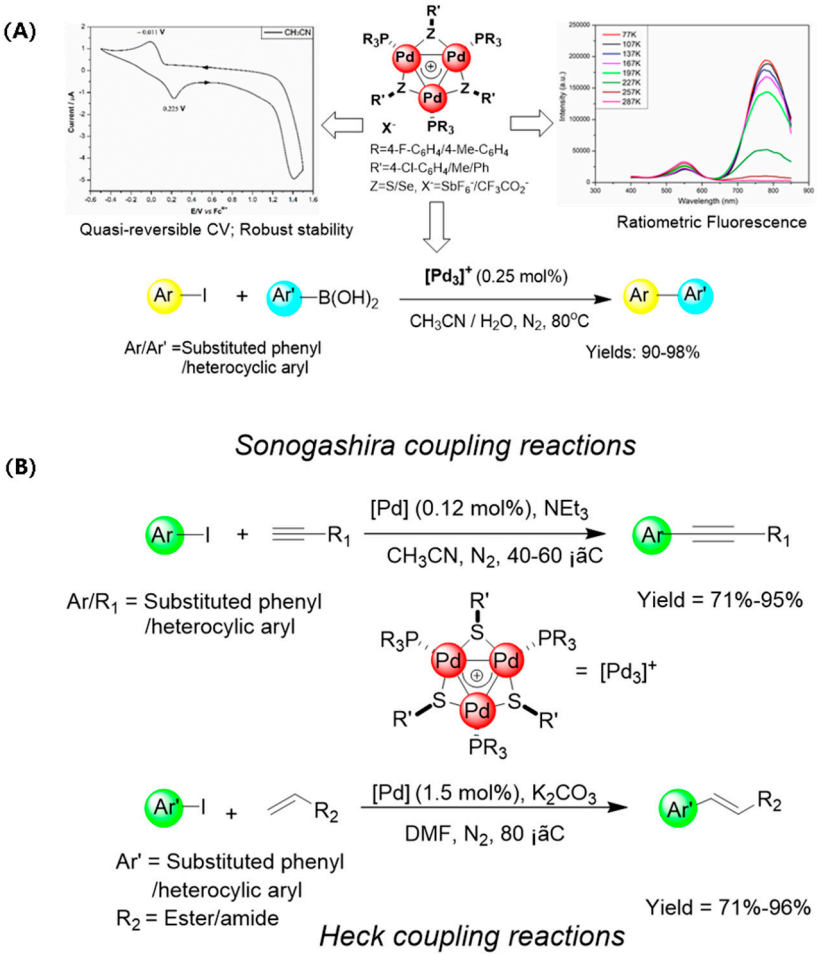

Figure 30. (**A**) Photoelectric properties and catalytic applications for S and aryl phosphine ligated aromatic triangular tri-palladium complexes $[Pd_3]^+$. Adapted with permission from ref. [152] Copyright © 2024, Royal Society of Chemistry. (**B**) Sulfur and aryl phosphine ligated $[Pd_3]^+$ clusters catalyzed Sonogashira and Heck coupling reactions. Adapted with permission from ref. [153] Copyright © 2024, Wiley-VCH Verlag GmbH & Co. KGaA, Weinheim, Germany.

5. Cation–π Interactions of Triangular All-Metal Aromatics

5.1. Coordination of Aromatic $[Pd_3]^+$ to Lewis Acids

Normally, delocalized bonds in main-group aromatics could play the roles as electron donors and form bonding interactions with Lewis-acid species. Indeed, the cation–π interactions are well documented for the main-group aromatics and they play a crucial role in chemistry and biology [154–156]. The sulfur atom and aryl phosphine ligand simultaneously stabilized tri-palladium complex $[Pd_3]^+$ has been proven to be aromatic using many types of physical measurements and theoretical calculations. For further extending the applications of $[Pd_3]^+$ in coordination, our group investigated the interactions of the aromatic $[Pd_3]^+$ molecule with a variety of Lewis acids, such as Li(I), Ag(I), Au(I) and Cu(I). With a similar interest, by means of DFT methods, Tsipis predicted the tendency and possibilities of interactions between the ligand-stabilized aromatic triangular gold

rings and Lewis acids years earlier [157]. As we know, Lewis acids are possible to form bonding interactions with main group arenes that possess a negative quadrupolar moment perpendicular to their plane (Q_{zz}) [158]. For comparison, the calculated Q_{zz} for cationic $[Pd_3]^+$ is −52 Buckingham, and the Q_{zz} of benzene is −8.5 Buckingham, and for hexafluorobenzene is +9.5 Buckingham (Figure 31). By the same calculation model, the calculated Q_{zz} values for the $[Pd_3]^+$ cations were seven times that of benzene. The largely negative values of aromatic $[Pd_3]^+$ suggested that these cationic clusters hold a strong possibility of forming bonding interactions with Lewis acids. However, to the best of our knowledge on heterometallics [159–162], there were no experimentally isolated complexes to confirm this conjecture.

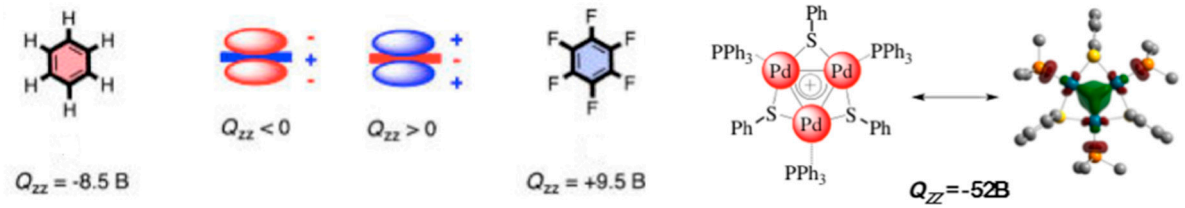

Figure 31. Calculated Quadrupole moments and ion affinities for representative main-group aromatics and aromatic triangular tripalladium cation $[Pd_3]^+$.

In 2017, we reported the first "pyramid" structure of $[Pd_3Ag]^{2+}$ formed by the coordination of the triangular all-metal aromatic $[Pd_3]^+$ and Lewis acid Ag^+ (Figure 32) [163]. Cationic $[Pd_3]^+$ can act as donor ligands thanks to their three-centre-two-electron metallic structure with delocalized metal–metal bonds. Driven by the cation–π interaction, the all-metal aromatic ligand $[Pd_3]^+$ and Lewis acid Ag^+ overcame the unavoidable electrostatic repulsions and formed these "peculiar" cation–cation-coordinated "pyramid" complexes. This result proved that parent all-metal aromatic complexes $[Pd_3]^+$ have the properties of aromatic rings that are crafted with main group elements. Echoed with their main group element counterparts and overcoming the electrostatic repulsions, these noble-metallic rings formed stable bonding interactions with several Lewis acids, such as Ag^+, Au^+, Cu^+, to deliver the corresponding tetranuclear bimetallic complexes with quantitative yields. These novel pyramid tetra-metal complexes $[Pd_3M]^{2+}$ were fully characterized including HRMS and single-crystal X-ray diffractions. Through comprehensive modelling and experimental techniques for these bimetallic clusters, it was concluded that this bonding mode in $[Pd_3Ag]^{2+}$ is an original coordination-like one rather than a four-centre-two-electron bond.

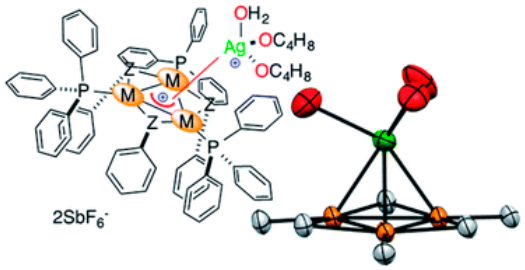

Figure 32. Interactions of all-metal aromatic cationic tri-palladium cores with Lewis acidic cation Ag^+. Adapted with permission from ref. [163] Copyright © 2024, Royal Society of Chemistry.

5.2. Coordination of π-Aromatic B_3^+ to Transition Metals

The triangular B_3 unit is a fundamental bonding template among all boron compounds. Previously isolated B_3^- cluster possessed a D_{3h} structure and had double (σ and π) aromaticity. Using computational chemistry and high-resolution photoelectron imaging, several chemists investigated the bonding modes between a B_3 cluster and metallic Lewis acids. For example, Boldyrev and Wang studied the IrB_3^- cluster via high-resolution photoelectron imaging and theoretical calculations. They experimentally observed two

isomers with different electron affinities and both structures had a B_3 ring coordinated with one Ir atom (Figure 33) [164]. The isomer with the higher EA consisted of one B_3 ring with a bridge-bonded Ir atom (C_s), and the isomer with the lower EA featured a tetrahedral structure (C_{3v}). Chemical bonding analyses showed that the neutral C_{3v} isomer could be viewed as an Ir–(η^3-B_3^+) complex, in which significant covalent bonding (Ir–B) and weak charge transfer from B_3 to Ir (ionic bonding) existed. The neutral tetrahedral structure was proved to be very stable. This study provided the experimental evidence and theoretical support for a π-aromatic B_3^+ ring coordinating with a Lewis acid or transition metal.

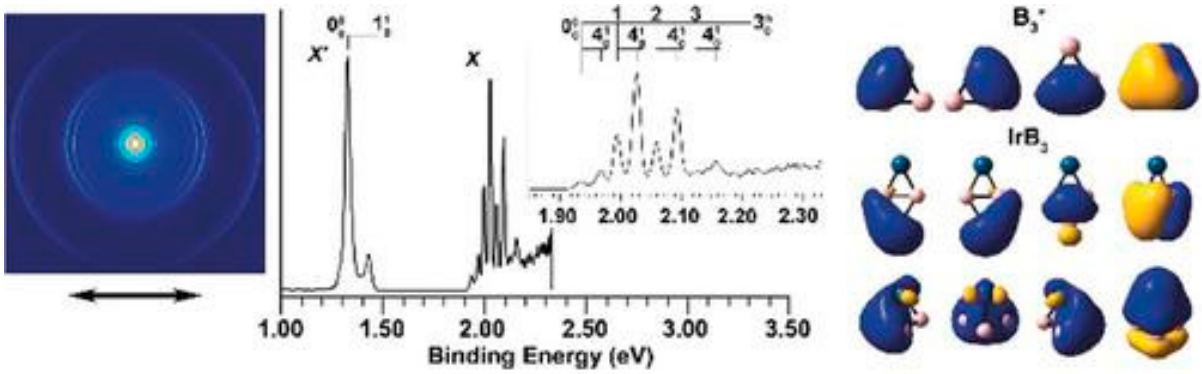

Figure 33. The high-resolution photoelectron image of complexed IrB_3^- structure proved the coordination of π-aromatic B_3^+ ring to the transition metal Ir. Adapted with permission from ref. [164] Copyright © 2024, Wiley-VCH Verlag GmbH & Co. KGaA, Weinheim, Germany.

In addition, Wang and colleagues investigated the high-resolution photoelectron imaging of MnB_3^- [165]. Theoretical calculation found that this is a C_{2v} planar structure in which the Mn is coordinated to only one side of the B_3 unit. The Mn atom showed weak interactions with the B_3 unit which still maintained the double aromaticity with small structural changes compared to the bare B_3 cluster. The present results thus pave the way for the use of suitable triangular all-metal rings as aromatic ligands for a variety of Lewis acids for cation–π interactions. It is anticipated that the introduction of aromatic all-metal cationic metallic rings as a new class of donor ligands is promising for vast innovation in coordination chemistry, materials, and catalysis [166–169].

6. Experimental and Theoretical Developments of Triangular All-Metal Aromatic Sandwiches

A sandwich structure usually means that one metal atom is bounded by two aromatic ligands like ferrocene, which was discovered at the beginning of metallocene chemistry. Now, it has been extended to include aromatic metallic ligands which could also be carbon-free as all-metal-containing layers [170]. In 2010, Fujita and coworkers reported the first three-dimensional all-metal aromatic complex in which metal ions were arrayed in a sandwich shape [171]. The planar polymetallic complexes could be coordinated and assembled as aromatic stacks. For the first time, a crystallographic X-ray of a trigonal prismatic cluster made of three cyclic triangular Au(I) layers was obtained (Figure 34a). By simply mixing the hexa-metallic Au_3-Au_3 complex with Ag(I) ion, the Ag-sandwiched complex Au_3-Ag-Au_3 could also be obtained. The composition of the initial polynuclear complexes and the shape of the yielded sandwiches determined the exact method of arrangement in the caged clusters (Figure 34b). In fact, based on triangular all-metal mono-layers, the preparation of all-metal aromatic sandwiches was an excellent breakthrough and opened the possibilities for their potential applications in material science as semiconductors.

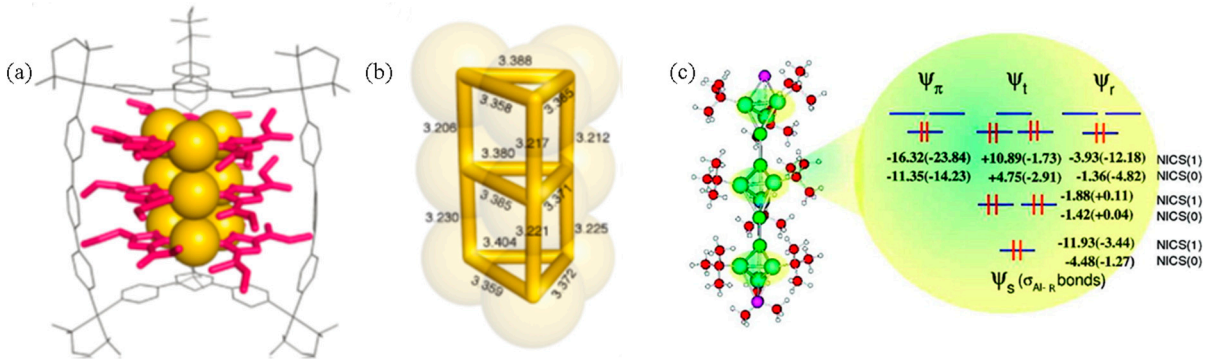

Figure 34. (**a**) X-ray crystal structure of the Au(I) sandwich; (**b**) Highlight of the trigonal prismatic structure for the three-layered Au(I) sandwich. The Au-Au bond lengths are given in Å. Adapted with permission from ref. [171] Copyright © 2024, American Chemical Society. (**c**) Structure and NICS values for sandwich complexes η^3-Al_3R_3. Adapted with permission from ref. [172] Copyright © 2024, American Chemical Society.

Besides experimental findings, there are also theoretical proofs for the existence of aromaticity in peculiar all-metal sandwiches. For example, some metallic sandwich complexes made of arraying aromatic triangular layer Al_3R_3 (perfluorinated cyclotrialane) were calculated by Mercero and coworkers. For better understanding, their structural and electronic properties were also investigated using density functional theory (Figure 34c) [172]. As we know, the perfluorinated cyclotrialane ring possesses both strong σ and π aromaticities, and it has been confirmed to be a very stable ligand for metal–ligand coordination during the sandwich formation process. In addition, with thorough theoretical calculations, the authors claimed that when the perfluorocyclotrialane ligands were employed to complex the other single metals or metal dimers, the aromaticity of the all-metal triangular ligand remained.

In 2015, Sun, Zhai and coworkers reported the synthesis and isolation of another all-metal aromatic sandwich complex, $[Sb_3Au_3Sb_3]^{3-}$, in which the structure and composition were confirmed by single-crystal X-ray diffraction (Figure 35a) [173]. Quantum chemical calculations demonstrated that there were obvious intramolecular electron transfers among the three all-metal layers. Their valence electrons were clearly rearranged from the cyclo-Sb_3 layers and Au_3 interlayers to the Au–Sb bonds. The whole triangular sandwich complex was combined via σ bonding. According to the reversed Hückel rule for aromaticity, the delocalization of the 3c–3e π bonds for each cyclo-Sb_3 layer proved the presence of aromaticity (Figure 35b,c). Theoretical studies on the electron structures and bonding forms of $[Au_3Sb_6]^{3-}$ were also carried out [174]. This new type of all-metal, aromatic sandwich complex was prospected to hold great potential in applications as semiconducting materials.

A short time later, Li and coworkers reported one similar D_{3h} symmetric all-metal aromatic sandwich structure, $[Bi_3Au_3Bi_3]^{3-}$; this species was investigated systematically via density functional theory (Figure 35d) [175]. Both molecular orbital analysis and nucleus-independent chemical shift data confirmed that similar to the cyclo-Sb_3 $[Sb_3Au_3Sb_3]^{3-}$ complex, cyclo-Bi_3 in $[Bi_3Au_3Bi_3]^{3-}$ possessed both σ and π aromaticities. However, the cyclo-Au_3 possessed σ and δ aromaticity and even weak π antiaromaticity. The authors analyzed the bonding nature of each type of bond in this sandwich complex and suggested that the Bi–Bi bond was a nonpolar σ covalent bond; the Au–Bi bond is a polar σ covalent bond; and the Au–Au bond was attributed to the typical aurophilic interaction. In addition, the intermolecular electron transfer phenomenon between cyclo-Au_3 and cyclo-Bi_3 was observed by charge decomposition analysis. Besides that, the robust stability of these complexes could be explained by their large E_{gap} and small $\Delta\, e^{avg}{}_R$ which also indicated their potential application as one new type of semiconductor material.

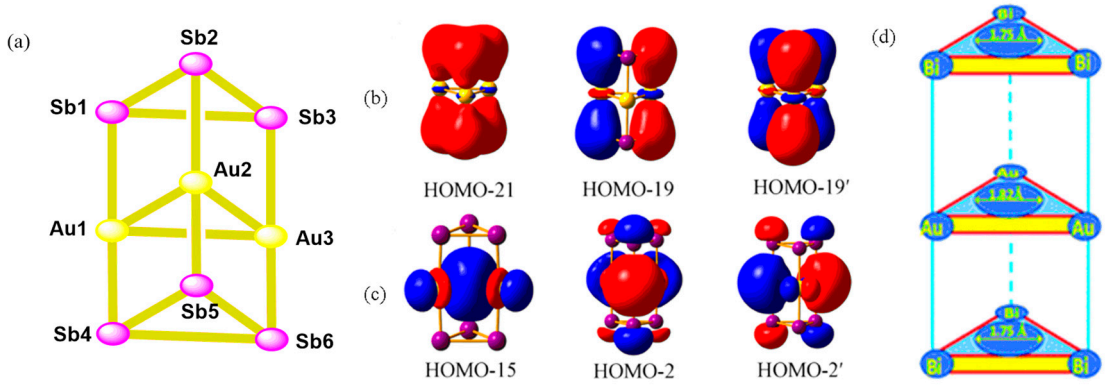

Figure 35. (**a**) Molecular structure for all-metal sandwich complex $[Sb_3Au_3Sb_3]^{3-}$. (**b**) HOMO-21 and HOMO-19/HOMO-19′ showed Sb → Au donation. (**c**) Au 6s-based molecular orbitals: HOMO-15 and HOMO-2/HOMO-2′. Adapted with permission from ref. [173] Copyright © 2024, American Chemical Society. (**d**) Structure of the all-metal aromatic sandwich structure $[Bi_3Au_3Bi_3]^{3-}$. Adapted with permission from ref. [175] Copyright © 2024, Royal Society of Chemistry.

Additionally, the φ-aromaticity for prismatic {Bi_6}-based clusters was also demonstrated [176]. The aromaticity, electronic structures, and interactions with hydrogens for all-metal aromatic binuclear sandwich complexes were further illustrated [177]. The all-metal binuclear sandwich clusters $Al_4Ti_2Al_4$ were proved to be high-capacity hydrogen storage structures through multicentre bonds [178]. The four-fold π/σ aromatic sandwich-type $Na_6B_7^-$ and $Na_8B_7^+$ complexes featured charge-transfer complexes [179]. Trinuclear mixed-metal sandwich complexes could also construct axially chiral metal skeletons by selective dimerization [180]. The coordination modes and ligand influences for cyclooctatetraene ligated trinuclear Pd3 sandwich complexes were theoretically investigated [181]. Trinuclear Pd metal sheet sandwich complexes have peculiar electronic structures and hold great potential for further functionalization [182].

7. Conclusions

Triangular all-metal aromatics are a group of organometallic complexes that possess the smallest ring and conform to the Hückel (4n + 2) rule with all-metal σ, π or δ-aromaticity among transition metals, semimetallics and other metals. These metallic clusters proved to be either analogues of the σ-aromatic molecules $[H_3]^+$ ion or analogues of the π-aromatic molecule's $[C_3H_3]^+$ ion. As summarized in the review, the syntheses, characterizations and theoretical calculations for isolated robust triangular all-metal aromatic clusters like $[Ga_3]^{2-}$, $[Al_3]^{2-}$, $[B_3]^{2-}$ $[Si]_3^+$, $[Ge]_3^+$, $[Au]_3^+$, $[Zn_3]^+$, $[Pd_3]^+$, $[Pt_3]^+$, $[Th_3]^+$, $[Pd_2Ru]^+$, $[Pd_2Pt]^+$ and $[PdPt_2]^+$ have been demonstrated. Theoretical calculations have predicted the existence of multiple types of aromaticity in proposed structures like $[M_3O_9]^-$ and $[M_3O_9]^{2-}$ (M = W, Mo), $[Ta_3O_3]^-$, $[Tc_3X_9]^{2-}$, $[Sc_3]^-$, $[Al_3]^-$, $[M_3]^{4+}$ (M = Ni, Pd, Pt), $[Hf_3]^+$, $Os_3N_3^{+/-}$, $Ir_3N_3^{+/-}$, and PrB_2^-. Experimental and theoretical developments of all-metal aromatics involved in sandwiches are well developed. The aromaticity of the all-metal triangular ligand in the sandwiches could also remain. The isolation of complex aromatic sandwiches will pave the way for the synthesis of entirely new classes of complexes and hold potential technological applications as semiconductors.

The first σ-aromatic cation $[Au_3]^+$ showed clear activity in the amine carbonylation reaction and provided modest yields. Comparatively, trinuclear all-metal aromatic $[Pd_3]^+$ proved to be a strong candidate for catalytic applications in several optimized catalytic systems like semi-reduction of internal alkynes to deliver *cis*-alkenes with almost complete selectivity on a gram scale with very low catalyst loadings. Powerful activity was also obtained in the cycloisomerization of terminal 1,6-enynes and internal dienynes under mild conditions and Suzuki–Miyaura, Sonogashira, and Heck C–C cross-coupling of aryl halides and arylboronic acids under mild conditions. By now, the all-metal aromatic

cationic metal rings were applied in coordination chemistry successfully and used as a new class of donor ligands for a variety of Lewis acids through cation–π interactions. This summarised review will propagate the importance and developments of triangular and sandwich-typed all-metal aromatics and the prospect that this group of peculiar structures could participate in more types of in-depth applications in coordination chemistry, catalysis, and material science.

Above all, many types of triangular and sandwich-typed all-metal aromatics were synthetically isolated or theoretically predicted, and the types of metals in three-membered circles possessing aromaticity were still very limited compared to the integral metal species on the periodical table. By now, besides the three-membered circles, larger aromatic circles (four-, five-, six-membered) composed of pure metals were rarely discovered. In fact, most of the successful syntheses originated from unexpected discoveries rather than purposeful preparations and most of the designed syntheses routes cannot be achieved due to their exclusive metallic properties and subtle coordination relationships with ligands. Besides the enthusiasm for their peculiar structures of triangular and sandwich-typed all-metal aromatics, their applications in coordination chemistry, catalysis, and material science could be developed and carried forward in the future decades.

Author Contributions: Conceptualization and methodology, M.W. and Y.W.; formal analysis, M.W.; writing—original draft preparation, M.W.; writing—review and editing, Y.W.; supervision and funding acquisition, Y.W. All authors have read and agreed to the published version of the manuscript.

Funding: This work was financially supported by the National Natural Science Foundation of China (Grant No. 21901097); Natural Science Foundation of Shandong Province (Grant No. ZR2023MB075); Liaocheng University Foundation (Grant No. 318051728); Introduction and Cultivation Program for Young Innovative Talents in Shandong Provincial Colleges and Universities (Innovation Team of Functional Organometallic Materials Presided by Yanlan Wang).

Institutional Review Board Statement: Not applicable.

Informed Consent Statement: Not applicable.

Data Availability Statement: No new data were created.

Conflicts of Interest: The authors declare that they have no known competing financial interests or personal relationships that could have appeared to influence the work in this paper.

References

1. Proft, F.D.; Geerlings, P. Conceptual and Computational DFT in the Study of Aromaticity. *Chem. Rev.* **2001**, *101*, 1451–1464. [CrossRef]
2. Kékule, A. Sur la constitution des substances aromatiques. *Bull. Soc. Chim. Fr.* **1865**, *3*, 98–110.
3. Popov, I.A.; Starikova, A.A.; Steglenko, D.V.; Boldyrev, A.I. Usefulness of the σ-Aromaticity and σ-Antiaromaticity Concepts for Clusters and Solid-State Compounds. *Chem. Eur. J.* **2018**, *24*, 292–305. [CrossRef] [PubMed]
4. Clark, E. *Polycyclic Hydrocarbons*; Academic Press: New York, NY, USA, 1964. [CrossRef]
5. Thorn, D.L.; Hoffmann, R. Delocalization in metallocycles. *Nouv. J. Chim.* **1979**, *3*, 39–45.
6. He, X.; Yu, D.; Wu, J.; Wang, B.; Rong, C.; Chattaraj, P.; Liu, S. Towards Understanding Metal Aromaticity in Different Spin States: A Density Functional Theory and Information-Theoretic Approach Analysis. *Chem. Phy. Lett.* **2020**, *761*, 138065. [CrossRef]
7. Hu, H.C.; Zhao, B. Metal-Organic Frameworks Based on Multicenter-Bonded $[M^I]_8$ (M = Mn, Zn) Clusters with Cubic Aromaticity. *Chem. Eur. J.* **2018**, *24*, 16702–16707. [CrossRef]
8. Bleeke, J.R. Metallabenzenes. *Chem. Rev.* **2001**, *101*, 1205–1228. [CrossRef]
9. Fernández, I.; Frenking, G.; Merino, G. Aromaticity of Metallabenzenes and Related Compounds. *Chem. Soc. Rev.* **2015**, *44*, 6452–6463. [CrossRef] [PubMed]
10. Tkachenko, N.V.; Popov, I.A.; Kulichenko, M.; Fedik, N.; Sun, Z.M.; Muñoz-Castro, A.; Boldyrev, A.I. Bridging Aromatic/Antiaromatic Units: Recent Advances in Aromaticity and Antiaromaticity in Main-Group and Transition-Metal Clusters from Bonding and Magnetic Analyses. *Eur. J. Inorg. Chem.* **2021**, *41*, 4239–4250. [CrossRef]
11. Bleeke, J.R. Aromatic iridacycles. *Acc. Chem. Res.* **2007**, *40*, 1035–1047. [CrossRef]
12. Wright, L.J. Metallabenzenes and metallabenzenoids. *Dalton Trans.* **2006**, 1821–1827. [CrossRef] [PubMed]
13. Lanford, C.W.; Haley, M.M. Recent advances in metallabenzene chemistry. *Angew. Chem. Int. Ed.* **2006**, *45*, 3914–3936. [CrossRef]
14. Boldyrev, A.I.; Wang, L.S. All-metal aromaticity and antiaromaticity. *Chem. Rev.* **2005**, *105*, 3716–3757. [CrossRef] [PubMed]

15. You, X.R.; Zhai, H.J. Can Synthetic All-Metal Cluster Compound Support Multifold (π and σ) Aromaticity and d-Orbital Aromaticity? *Chin. J. Chem.* **2019**, *37*, 126–130. [CrossRef]
16. Chen, Z.; Wannere, C.S.; Corminboent, C.; Puchta, R.; von R. Schleyer, P. Nucleus-independent chemical shifts (NICS) as an aromaticity criterion. *Chem. Rev.* **2005**, *105*, 3842–3888. [CrossRef]
17. von Ragué Schleyer, P.; King, R.B. Aromaticity of Tri-and Tetranuclear Metal–Carbonyl Clusters Based on Magnetic Criteria. *Chem. Eur. J.* **2007**, *13*, 978–984. [CrossRef]
18. Paul, S.; Misra, A. Interplay among Aromaticity, Magnetism, and Nonlinear Optical Response in All-Metal Aromatic Systems. *Inorg. Chem.* **2011**, *50*, 3234–3246. [CrossRef]
19. Mercero, J.M.; Boldyrev, A.I.; Merino, G.J.M.; Ugalde, J.M. Recent developments and future prospects of all-metal aromatic compounds. *Chem. Soc. Rev.* **2015**, *44*, 6519–6534. [CrossRef]
20. Chen, D.; Hua, Y.; Xia, H. Metallaaromatic Chemistry: History and Development. *Chem. Rev.* **2020**, *120*, 12994–13086. [CrossRef]
21. Poater, J.; Solà, M. Open-Shell Jellium Aromaticity in Metal Clusters. *Chem. Commun.* **2019**, *55*, 5559–5562. [CrossRef]
22. Chen, D.; Xie, Q.; Zhu, J. Unconventional Aromaticity in Organometallics: The Power of Transition Metals. *Acc. Chem. Res.* **2019**, *52*, 1449. [CrossRef]
23. Jr, J.H.D.; Rabelo, J.N.T.; Candido, L. Electron Correlation Effects in All-Metal Aromatic Clusters: A Quantum Monte Carlo Study. *Inorg. Chem.* **2016**, *55*, 7442–7447. [CrossRef]
24. Bigi, F.; Cera, G.; Maggi, R.; Wang, Y.; Malacria, M.; Maestri, G. Is Aromaticity a Driving Force in Catalytic Cycles? A Case from the Cycloisomerization of Enynes Catalyzed by All-Metal Aromatic Pd_3^+ Clusters and Carboxylic Acids. *J. Phys. Chem. A* **2021**, *125*, 10035–10043. [CrossRef]
25. Bigi, F.; Cauzzi, D.; Della Ca, N.; Malacria, M.; Maggi, R.; Motti, E.; Wang, Y.; Maestri, G. Evolution of Triangular All-Metal Aromatic Complexes from Bonding Quandaries to Powerful Catalytic Platforms. *ACS Org. Inorg. Au* **2022**, *2*, 373–385. [CrossRef]
26. Alexandrova, A.N.; Boldyrev, A.I. σ-Aromaticity and σ-antiaromaticity in alkali metal and alkaline earth metal small clusters. *J. Phys. Chem. A* **2003**, *107*, 554–560. [CrossRef]
27. Tsipis, C.A. DFT study of "all-metal" aromatic compounds. *Coord. Chem. Rev.* **2005**, *249*, 2740–2762. [CrossRef]
28. Huang, X.; Zhai, H.J.; Kiran, B.; Wang, L.-S. Observation of d-orbital aromaticity. *Angew. Chem. Int. Ed.* **2005**, *44*, 7251–7254. [CrossRef] [PubMed]
29. Feixas, F.; Matito, E.; Poater, J.; Solà, M. Quantifying aromaticity with electron delocalisation measures. *Chem. Soc. Rev.* **2015**, *44*, 6434–6451. [CrossRef] [PubMed]
30. Alvarado-Soto, L.; Ramírez-Tagle, R.; Arratia-Pérez, R. Spin–orbit effects on the aromaticity of the Re_3Cl_9 and Re_3Br_9 clusters. *Chem. Phys. Lett.* **2008**, *467*, 94–96. [CrossRef]
31. Zhai, H.J.; Wang, B.; Huang, X.; Wang, L.S. Probing the Electronic and Structural Properties of the Niobium Trimer Cluster and Its Mono-and Dioxides: $Nb_3O_n^-$ and Nb_3O_n (n = 0–2). *J. Phys. Chem. A* **2009**, *113*, 3866–3875. [CrossRef]
32. Alvarado-Soto, L.; Ramírez-Tagle, R.; Arratia-Pérez, R. Spin-Orbit Effects on the Aromaticity of the $Re_3X_9^{2-}$(X = Cl, Br) Cluster Ions. *J. Phys. Chem. A* **2009**, *113*, 1671–1673. [CrossRef]
33. Sergeeva, A.P.; Boldyrev, A.I. The Chemical bonding of Re_3Cl_9 and revealed by the adaptive natural density partitioning analyses. *Inorg. Chem.* **2010**, *31*, 2–12. [CrossRef]
34. Hirschfelder, J.O. The energy of the triatomic hydrogen molecule and ion. *J. Chem. Phys.* **1938**, *6*, 795–806. [CrossRef]
35. Radom, L.; Hariharan, P.C.; Pople, J.A.; Schleyer, P.v.R. Molecular orbital theory of the electronic structure of organic compounds. XXII. Structures and stabilities of $C_3H_3^+$ and C_3H^+ cations. *J. Am. Chem. Soc.* **1976**, *98*, 10–14. [CrossRef]
36. Twamley, B.; Power, P.P. Synthesis of the Square-Planar Gallium Species $K_2[Ga_4(C_6H_3$-2, 6-$Trip_2)_2]$(Trip=C_6H_2-2, 4, 6-*i*Pr_3): The Role of Aryl–Alkali Metal Ion Interactions in the Structure of Gallium Clusters. *Angew. Chem. Int. Ed.* **2000**, *39*, 3500–3502. [CrossRef]
37. Wiberg, N.; Blank, T.; Westerhausen, M.; Schneiderbauer, S.; Schnöckel, H.; Krossing, I.; Schnepf, A. Disodium Tetrasupersilyltetragallanediide $Na_2Ga_4R^*_4\cdot$ 2THF (R*= $SitBu_3$)—Preparation of a Novel Gallium Cluster Compound via Dichlorodisupersilyldigallane R*2Ga_2Cl_2. *Eur. J. Inorg. Chem.* **2002**, *2002*, 351–356. [CrossRef]
38. Hoffmann, R. The many guises of aromaticity. *Am. Sci.* **2015**, *103*, 18–22. [CrossRef]
39. Li, X.W.; Pennington, W.T.; Robinson, G.H. Metallic system with aromatic character. synthesis and molecular structure of Na_2[[(2, 4, 6-$Me_3C_6H_2)_2C_6H_3$]Ga]$_3$ the first cyclogallane. *J. Am. Chem. Soc.* **1995**, *117*, 7578–7579. [CrossRef]
40. Lichtenthaler, M.; Stahl, F.; Kratzert, D.; Heidinger, L.; Schleicher, E.; Hamann, J.; Himmel, D.; Weber, S.; Krossing, I. Cationic cluster formation versus disproportionation of low-valent indium and gallium complexes of 2,2′-bipyridine. *Nat. Commun.* **2015**, *6*, 8288. [CrossRef] [PubMed]
41. Wang, Y.; Robinson, G.H. Organometallics of the Group 13 M–M Bond (M = Al, Ga, In) and the Concept of Metalloaromaticity. *Organometallics* **2007**, *26*, 2–11. [CrossRef]
42. Li, X.W.; Xie, Y.; Schreiner, P.R.; Gripper, K.D.; Crittendon, R.C.; Campana, C.F.; Schaefer, H.F.; Robinson, G.H. Cyclogallanes and metalloaromaticity. Synthesis and molecular structure of dipotassium tris ((2,6-dimesitylphenyl) cyclogallene), $K_2[(Mes_2C_6H_3)Ga]_3$ (Mes = 2,4,6-$Me_3C_6H_2$): A structural and theoretical examination. *Organometallics* **1996**, *15*, 3798–3803. [CrossRef]
43. Xie, Y.; Schreiner, P.R.; Schaefer, H.F.; Li, X.W.; Robinson, G.H. Are Cyclogallenes [M_2 $(GaH)_3$](M = Li, Na, K) Aromatic? *J. Am. Chem. Soc.* **1996**, *118*, 10635–10639. [CrossRef]

44. Xie, Y.; Schreiner, P.R.; Schaefer, H.F.; Li, X.W.; Robinson, G.H. Are Heterocyclic 2π-Electron Aromatic Systems HC–Ga(H)–CH, M[HGa–C(H)–GaH], $[HGa–C(H)–GaH]^-$, HSi–Ga(H)–SiH, M[HGa–Si(H)–GaH](M = Li, Na, and K), and $[HGa–Si(H)–GaH]^-$ Stable? *Organometallics* **1998**, *17*, 114–122. [CrossRef]
45. Robinson, G.H. Gallanes, gallenes, cyclogallenes, and gallynes: Organometallic chemistry about the gallium–gallium bond. *Acc. Chem. Res.* **1999**, *32*, 773–782. [CrossRef]
46. Wright, R.J.; Brynda, M.; Power, P.P. Synthesis and Structure of the "Dialuminyne" $Na_2[Ar' AlAlAr']$ and $Na_2[(Ar'' Al)_3]$: Al-Al Bonding in Al_2Na_2 and Al_3Na_2 Clusters. *Angew. Chem. Int. Ed.* **2006**, *45*, 5953–5956, Version *Angew. Chem.* **2006**, *118*, 6099–6102. [CrossRef] [PubMed]
47. Kupfer, T.; Braunschweig, H.; Radacki, K. The Triboracyclopropenyl Dianion: The Lightest Possible Main-Group-Element Hückel π Aromatic. *Angew. Chem. Int. Ed.* **2015**, *54*, 15084–15088. [CrossRef] [PubMed]
48. Li, N.; Wu, B.; Yu, C.; Li, T.; Zhang, W.; Xi, Z. Trishomoaromatic ($B_3N_3Ph_6$)-Dianion: Characterization and Two-Electron Reduction. *Angew. Chem. Int. Ed.* **2020**, *59*, 8868–8872. [CrossRef] [PubMed]
49. Jin, J.; Wang, G.; Zhou, M.; Andrada, D.; Hermann, M.; Frenking, G. The $[B_3(NN)_3]^+$ and $[B_3(CO)_3]^+$ Complexes Featuring the Smallest π-Aromatic Species B_3^+. *Angew. Chem.* **2016**, *128*, 2118–2122. [CrossRef]
50. Saha, R.; Pan, S.; Mandal, S.; Orozco, M.; Merino, G.; Chattaraj, P. Noble gas supported B_3^+ cluster: Formation of strong covalent noble gas–boron bonds. *RSC Adv.* **2016**, *6*, 78611–78620. [CrossRef]
51. Zhang, R.; Li, A.; Li, Z. Circular cationic compounds $B_3Rg_n^+$ of triangular ion B_3^+ trapping rare gases. *Chem. Res. Chin. Univ.* **2017**, *33*, 958–964. [CrossRef]
52. Kuznetsov, A.E.; Boldyrev, A.I. Theoretical Evidence of Aromaticity in X_3^- (X = B, Al, Ga) Species. *Struct. Chem.* **2002**, *13*, 141–148. [CrossRef]
53. Ullah, S.; Mazumder, L.; Kaushik, S.; Das, N.; Brahma, M.; Sharma, P.; Guha, A. Electronic Structure, Stability, and Aromaticity of H_2B_2XH (X = N, P) molecules: A Theoretical Study. Comput. *Theor. Chem.* **2017**, *1113*, 120–125. [CrossRef]
54. Cheung, L.F.; Kocheril, G.S.; Czekner, J.; Wang, L.S. Observation of Möbius Aromatic Planar Metallaborocycles. *J. Am. Chem. Soc.* **2020**, *142*, 3356–3360. [CrossRef] [PubMed]
55. Alexandrova, A.N.; Boldyrev, A.I.; Zhai, H.J.; Wang, L.S. All-Boron Aromatic Clusters as Potential New Inorganic Ligands and Building Blocks in Chemistry. *Coord. Chem. Rev.* **2006**, *250*, 2811–2866. [CrossRef]
56. Jemmis, E.D.; Srinivas, G.N.; Leszczynski, J.; Kapp, J.; Korkin, A.A.; von R. Schleyer, P. Group 14 analogs of the cyclopropenium ion: Do they favor classical aromatic structures? *J. Am. Chem. Soc.* **1995**, *117*, 11361–11362. [CrossRef]
57. Cheng, N.; Liu, Y.; Zhang, C. Theoretical studies of traditional and halogen-shared halogen bonds: The doped all-metal aromatic clusters MAl_3^- (M = Si, Ge, Sn, Pb) as halogen bond acceptors. *Theor. Chem. Acc.* **2015**, *134*, 140. [CrossRef]
58. Li, J.; Wang, J.; Chen, J.; Bu, Y.; Cheng, S. Observation of "Outlaw" Dual Aromaticity in Unexpectedly Stable Open-Shell Metal Clusters Caused by Near-Degenerate Molecular Orbital Coupling. *CCS Chem.* **2020**, *2*, 1913–1920. [CrossRef]
59. Lee, V.Y.; Sekiguchi, A. Aromaticity of group 14 organometallics: Experimental aspects. *Angew. Chem. Int. Ed.* **2007**, *46*, 6596–6620. [CrossRef]
60. Kar, S.; Chatterjee, D.; Halet, J.; Ghosh, S. Trimetallic Chalcogenide Species: Synthesis, Structures, and Bonding. *Molecules* **2022**, *27*, 7473. [CrossRef]
61. Sekiguchi, A.; Tsukamoto, M.; Ichinohe, M.A. A free cyclotrigermenium cation with a 2π-electron system. *Science* **1997**, *275*, 60–61. [CrossRef]
62. Ichinohe, M.; Igarashi, M.; Sanuki, K.; Sekiguchi, A. Cyclotrisilenylium ion: The persilaaromatic compound. *J. Am. Chem. Soc.* **2005**, *127*, 9978–9979. [CrossRef]
63. Igarashi, M.; Ichinohe, M.; Sekiguchi, A. Air-Stable Disilacyclopropene with a Si-C Bond and Its Conversion to Disilacyclopropenylium Ion: Silicon–Carbon Hybrid 2π-Electron Systems. *J. Am. Chem. Soc.* **2007**, *129*, 12660–12661. [CrossRef]
64. Kuwabara, T.; Guo, H.D.; Nagase, S.; Saito, M. Diversity of the Structures in a Distannene Complex and its Reduction to Generate a Six-Membered Ti_2Sn_4 Ring Complex. *Angew. Chem. Int. Ed.* **2014**, *53*, 434–438, Version *Angew. Chem.* **2014**, *126*, 444–448. [CrossRef]
65. Pan, F.; Xu, C.; Li, L.; Min, X.; Wang, J.; Li, J.; Zhai, H.; Sun, Z. A niobium-necked cluster $[As_3Nb(As_3Sn_3)]^{3-}$ with aromatic Sn_3^{2-}. *Dalton Trans.* **2016**, *45*, 3874–3879. [CrossRef]
66. Robilotto, T.J.; Bacsa, J.; Gray, T.G.; Sadighi, J.P. Synthesis of a trigold monocation: An isolobal analogue of $[H_3]^+$. *Angew. Chem. Int. Ed.* **2012**, *51*, 12077–12080, Version *Angew. Chem.* **2012**, *124*, 12243–12246. [CrossRef]
67. Jin, L.; Weinberger, D.S.; Melaimi, M.; Moore, C.E.; Rheingold, A.L.; Bertrand, G. Trinuclear gold clusters supported by cyclic (alkyl)(amino) carbene ligands: Mimics for gold heterogeneous catalysts. *Angew. Chem. Int. Ed.* **2014**, *53*, 9059–9063. [CrossRef]
68. Freitag, K.; Gemel, C.; Jerabek, P.; Oppel, M.I.; Seidel, R.W.; Frenking, G.; Banh, H.; Dilchert, K.; Fischer, R.A. The σ-Aromatic Clusters $[Zn_3]^+$ and $[Zn_2Cu]$: Embryonic Brass; Version. *Angew. Chem. Int. Ed.* **2015**, *54*, 4370–4374, Version *Angew. Chem.* **2015**, *127*, 4445–4449. [CrossRef]
69. Banh, H.; Hornung, J.; Kratz, T.; Gemel, C.; Pöthig, A.; Gam, F.; Kahlal, S.; Saillard, J.Y.; Fischer, R.A. Embryonic Brass: Pseudo Two Electron Cu/Zn Clusters. *Chem. Sci.* **2018**, *9*, 8906–8913. [CrossRef]
70. Resa, I.; Carmona, E.; Gutierrez-Puebla, E.; Monge, A. Decamethyldizincocene, a stable compound of Zn (I) with a Zn-Zn bond. *Science* **2004**, *305*, 1136–1138. [CrossRef]

71. Zhao, Y.; Truhlar, D.G. A new local density functional for main-group thermochemistry, transition metal bonding, thermochemical kinetics, and noncovalent interactions. *J. Chem. Phys.* **2006**, *125*, 194101–194117. [CrossRef] [PubMed]
72. Weigend, F.; Ahlrichs, R.; Weigend, F.; Ahlrichs, R. Balanced basis sets of split valence, triple zeta valence and quadruple zeta valence quality for H to Rn: Design and assessment of accuracy. *Phys. Chem. Chem. Phys.* **2005**, *7*, 3297–3305. [CrossRef]
73. Mühlecker-Knoepfler, A.; Ellmerer-Muller, E.; Konrat, R.; Ongania, K.H.; Wurst, K.; Peringer, P.J. Synthesis and crystal structure of the subvalent mercury cluster [triangulo-Hg_3(μ-dmpm)$_4$][O_3SCF_3]$_4$ (dmpm = $Me_2PCH_2PMe_2$). *Chem. Soc. Dalton Trans.* **1997**, 1607–1610. [CrossRef]
74. Hämmerle, B.; Müller, E.P.; Wilkinson, D.L.; Muüller, G.; Peringer, P. Synthesis and structure of bis[sulphato]tris[μ-bis(diphenylphosphino) methane]-triangulo-trimercury. *J. Chem. Soc. Chem. Commun.* **1989**, 1527–1528. [CrossRef]
75. Blanchard, S.; Fensterbank, L.; Gontard, G.; Lacôte, E.; Maestri, G.; Malacria, M. Synthesis of triangular tripalladium cations as noble-metal analogues of the cyclopropenyl cation. *Angew. Chem. Int. Ed.* **2014**, *53*, 1987–1991, Version *Angew. Chem.* **2014**, *126*, 2018–2022. [CrossRef]
76. Wang, Y.; Deyris, P.A.; Caneque, T.; Blanchard, F.; Li, Y.; Bigi, F.; Maggi, R.; Blanchard, S.; Maestri, G.; Malacria, M. A Simple Synthesis of Triangular All-Metal Aromatics Allowing Access to Isolobal All-Metal Heteroaromatics. *Chem. Eur. J.* **2015**, *21*, 12271–12274. [CrossRef]
77. Albrecht, C.; Schwieger, S.; Bruhn, C.; Wagner, C.; Kluge, R.; Schmidt, H.; Steinborn, D.A. Alkylthio bridged 44 cve triangular platinum clusters: Synthesis, oxidation, degradation, ligand substitution, and quantum chemical calculations. *J. Am. Chem. Soc.* **2007**, *129*, 4551–4566. [CrossRef]
78. Murahashi, T.; Usui, K.; Tachibana, Y.; Kimura, S.; Ogoshi, S. Selective Construction of Pd_2Pt and $PdPt_2$ Triangles in a Sandwich Framework: Carbocyclic Ligands as Scaffolds for a Mixed-Metal System. *Chem. Eur. J.* **2012**, *18*, 8886–8890. [CrossRef]
79. Weinhold, F.; Landis, C.R. Natural bond orbitals and extensions of localized bonding concepts. *Chem. Educ. Res. Pract. Eur.* **2001**, *2*, 91–104. [CrossRef]
80. Zubarev, D.Y.; Boldyrev, A.I. Developing paradigms of chemical bonding: Adaptive natural density partitioning. *Phys. Chem. Chem. Phys.* **2008**, *10*, 5207–5217. [CrossRef]
81. Aihara, J. Circuit resonance energy: A key quantity that links energetic and magnetic criteria of aromaticity. *J. Am. Chem. Soc.* **2006**, *128*, 2873–2879. [CrossRef] [PubMed]
82. Proft, F.; von R. Schleyer, P.; Lenthe, J.H.; Stahl, F.; Geerlings, P. Magnetic Properties and Aromaticity of *o*-, *m*-, and *p*-Benzyne. *Chem. Eur. J.* **2002**, *8*, 3402–3410. [CrossRef]
83. Katritzky, A.R.; Barczynski, P.; Musumarra, G.; Pisano, D.; Szafran, M. Aromaticity as a quantitative concept. 1. A statistical demonstration of the orthogonality of classical and magnetic aromaticity in five-and six-membered heterocycles. *J. Am. Chem. Soc.* **1989**, *111*, 7–15. [CrossRef]
84. Kulichenko, M.; Fedik, N.; Monfredini, A.; Muñoz-Castro, A.; Balestri, D.; Boldyrev, A.I.; Maestri, G. "Bottled" spiro-doubly aromatic trinuclear $[Pd_2Ru]^+$ complexes. *Chem. Sci.* **2021**, *12*, 477–486. [CrossRef]
85. Boronski, J.T.; Seed, J.A.; Hunger, D.; Woodward, A.W.; van Slageren, J.; Wooles, A.J.; Natrajan, L.S.; Kaltsoyannis, N.; Liddle, S.T. A Crystalline Tri-Thorium Cluster with σ-Aromatic Metal–Metal Bonding. *Nature* **2021**, *598*, 75. [CrossRef]
86. Cuyacot, B.J.R.; Foroutan-Nejad, C. $[\{Th(C_8H_8)Cl_2\}_3]^{2-}$ is stable but not aromatic. *Nature* **2022**, *603*, E18. [CrossRef]
87. Chen, W.J.; Zhai, H.J.; Zhang, Y.F.; Huang, X.; Wang, L.S. On the Electronic and Structural Properties of Tri-Niobium Oxide Clusters $Nb_3O_n^-$ (n = 3–8): Photoelectron Spectroscopy and Density Functional Calculations. *J. Phys. Chem. A* **2010**, *114*, 5958–5966. [CrossRef]
88. Weck, P.F.; Sergeeva, A.P.; Kim, E.; Boldyrev, A.I.; Czerwinski, K.R. Chemical bonding and aromaticity in trinuclear transition-metal halide clusters. *Inorg. Chem.* **2011**, *50*, 1039–1046. [CrossRef]
89. Galeev, T.R.; Boldyrev, A.I. Recent advances in aromaticity and antiaromaticity in transition-metal systems. *Annu. Rep. Prog. Chem. Sect. C Phys. Chem.* **2011**, *107*, 124–147. [CrossRef]
90. Ivanov, A.S.; Zhang, X.; Wang, H.; Boldyrev, A.I.; Gantefoer, G.; Bowen, K.H.; Cernusak, I. Anion photoelectron spectroscopy and CASSCF/CASPT2/RASSI study of La_n^- (*n* = 1, 3–7). *J. Phys. Chem. A* **2015**, *119*, 11293–11303. [CrossRef]
91. Vásquez-Espinal, A.; Pino-Rios, R.; Alvarez-Thon, L.; Rabanal-León, W.A.; Torres-Vega, J.J.; Arratia-Perez, R.; Tiznado, W. New Insights into Re_3(μ-Cl)$_3Cl_6$ Aromaticity. Evidence of σ-and π-Diatropicity. *J. Phys. Chem. Lett.* **2015**, *6*, 4326–4330. [CrossRef]
92. Boldyrev, A.I.; Wang, L.S. Beyond organic chemistry: Aromaticity in atomic clusters. *Phys. Chem. Chem. Phys.* **2016**, *18*, 11589–11605. [CrossRef]
93. von R. Schleyer, P.; Maerker, C.; Dransfeld, A.; Jiao, H.; Eikema Hommes, N.J.R. Nucleus-independent chemical shifts: A simple and efficient aromaticity probe. *J. Am. Chem. Soc.* **1996**, *118*, 6317–6318. [CrossRef]
94. Li, X.; Kuznetsov, A.E.; Zhang, H.F.; Boldyrev, A.I.; Wang, L.S. Observation of all-metal aromatic molecules. *Science* **2001**, *291*, 859–861. [CrossRef]
95. Frenking, G. Building a quintuple bond. *Science* **2005**, *310*, 796–797. [CrossRef]
96. Radius, U.; Breher, F. To boldly pass the metal–metal quadruple bond. *Angew. Chem. Int. Ed.* **2006**, *45*, 3006–3010, Version *Angew. Chem.* **2006**, *118*, 3072–3077. [CrossRef]
97. Brynda, M.; Gagliardi, L.; Widmark, P.O.; Power, P.P.; Roos, B.O. A Quantum Chemical Study of the Quintuple Bond between Two Chromium Centers in [PhCrCrPh]: Trans-Bent versus Linear Geometry. *Angew. Chem.* **2006**, *118*, 3888–3891, Version *Angew. Chem. Int. Ed.* **2006**, *45*, 3804–3807. [CrossRef]

98. Zhai, H.; Averkiev, B.B.; Zubarev, D.Y.; Wang, L.S.; Boldyrev, A.I. δ Aromaticity in $[Ta_3O_3]^-$. *Angew. Chem.* **2007**, *119*, 4355–4358. [CrossRef]
99. Wang, L.S.; Wu, H. *Advances in Metaland Semiconductor Clusters, IV*; Cluster, Materials; Duncan, M.A., Ed.; JAI: Greenwich, CT, USA, 1998; pp. 299–343.
100. Badri, Z.; Pathak, S.; Fliegl, H.; Rashidi-Ranjbar, P.; Bast, R.; Marek, R.; Foroutan-Nejad, C.; Ruud, K. All-metal aromaticity: Revisiting the ring current model among transition metal clusters. *J. Chem. Theory Comput.* **2013**, *9*, 4789–4796. [CrossRef]
101. Mercero, J.M.; Matito, E.; Ruiperez, F.; Infante, I.; Lopez, X.; Ugalde, J.M. The Electronic Structure of the Al_3^- Anion: Is it Aromatic? *Chem. Eur. J.* **2015**, *21*, 9610–9614. [CrossRef]
102. Chen, J.; Yang, H.; Wang, J.; Cheng, S. Theoretical investigations on the d-p hybridized aromaticity, photoelectron spectroscopy and neutral salts of the LaX_2^- (X = Al, Ga, In) clusters. *Spectrochim. Acta Part A* **2018**, *203*, 132–138. [CrossRef]
103. Yang, H.; Wu, D.; He, H.; Yu, D.; Li, Y.; Li, Z. The behavior of the aluminum trimer when combining with different superatom clusters. *RSC Adv.* **2018**, *8*, 6667–6674. [CrossRef]
104. Xu, C.Q.; Xing, D.H.; Xiao, H.; Li, J. Manipulating stabilities and catalytic properties of trinuclear metal clusters through tuning the chemical bonding: H_2 adsorption and activation. *J. Phys. Chem. C* **2017**, *121*, 10992–11001. [CrossRef]
105. Reid, S.; Hernández, H. Characterization of the Effects of Ligands on Bonding and σ-Aromaticity of Small Pt Nanoclusters. *J. Phys. Chem. A* **2023**, *127*, 4237–4244. [CrossRef]
106. Ishikawa, Y.; Kimura, S.; Takase, K.; Yamamoto, K.; Kurashige, Y.; Yanai, T.; Murahashi, T. Modulation of Benzene or Naphthalene Binding to Palladium Cluster Sites by the Backside-Ligand Effect. *Angew. Chem. Int. Ed.* **2015**, *54*, 2482–2486. [CrossRef]
107. Link, H.; Reiss, P.; Chitsaz, S.; Pfistner, H.; Fenske, D. Synthese und Molekülstrukturen von amido-und imidoverbrückten Clustern elektronenreicher Übergangsmetalle. *Z. Für Anorg. Und Allg. Chem.* **2003**, *629*, 755–768. [CrossRef]
108. Lee, S.W.; Trogler, W.C. Synthesis and structure of the trinuclear palladium cluster $[Pd_3(PEt_3)_3\ (\mu_2\text{-NPh})_2(\mu_2\text{-NHPh})]Cl$, containing bridging imido and amido ligands. *Inorg. Chem.* **1990**, *29*, 1099–1102. [CrossRef]
109. Averkiev, B.B.; Boldyrev, A.I. Hf_3 Cluster Is Triply (σ-, π-, and δ-) Aromatic in the Lowest D_{3h}, $^1A_1'$ State. *J. Phys. Chem. A* **2007**, *111*, 12864–12866. [CrossRef]
110. Jin, Q.; Jin, B.; Jin, F.-K.; Li., J.-P. Theoretical evidence of triple (σ-, π-, and δ-) aromaticity in the $Os_3N_3^{+/-}$ clusters. *Comput. Thero. Chem.* **2017**, *1101*, 127–131. [CrossRef]
111. Jin, Q.; Jin, B.; Gong, L.; Jin, F. Aromaticity of the bare osmium trimers and the bindings to group IA/IIA all-metal series. *Comput. Theor. Chem.* **2017**, *1102*, 74–79. [CrossRef]
112. Jin, Q.; Jin, B.; Jin, Y.; Ding, H. On the electronic structures and multiple aromaticity in the $Ir_3N_3^{2+/0/2-}$ clusters and the $Ir_3N_3M^{-/0}$ or $Ir_3N_3M_2$ complexes with group IA/IIA metals. *Comput. Theor. Chem.* **2017**, *1118*, 75–80. [CrossRef]
113. Wang, Z.; Chen, T.; Chen, W.; Li, W.; Zhao, J.; Jiang, X.; Li, J.; Wang, L.; Hu, H. The smallest 4f-metalla-aromatic molecule of cyclo-PrB_2^- with Pr-B multiple bonds. *Chem. Sci.* **2022**, *13*, 10082–10094. [CrossRef]
114. Havenith, R.W.A.; Proft, F.; Fowler, P.W.; Geerlings, P. σ-Aromaticity in H_3^+ and Li_3^+: Insights from ring-current maps. *Chem. Phys. Lett.* **2005**, *407*, 391–396. [CrossRef]
115. Park, J.; Yoon, J.; Chung, Y. Cobalt/Rhodium Heterobimetallic Nanoparticle-Catalyzed Oxidative Carbonylation of Amines in the Presence of Carbon Monoxide and Molecular Oxygen to Ureas. *Adv. Synth. Catal.* **2009**, *351*, 1233–1237. [CrossRef]
116. Shelton, P.; Zhang, Y.; Nguyena, T.; McElwee-White, L. $NaIO_4$-oxidized carbonylation of amines to ureas. *Chem. Commun.* **2009**, 947–949. [CrossRef]
117. Díaz, D.; Darko, A.; McElwee-White, L. Transition Metal-Catalyzed Oxidative Carbonylation of Amines to Ureas. *Eur. J. Org. Chem.* **2007**, *2007*, 4453–4465. [CrossRef]
118. Gabriele, B.; Salerno, G.; Costa, M. Reviews. In *Catalytic Carbonylation Reactions*; Beller, M., Ed.; Springer: Berlin/Heidelberg, Germany, 2006; pp. 239–272.
119. Ragaini, F. Away from phosgene: Reductive carbonylation of nitroarenes and oxidative carbonylation of amines, understanding the mechanism to improve performance. *Dalton Trans.* **2009**, *32*, 6251–6266. [CrossRef]
120. Hashmi, A.S.K. Sub-nanosized gold catalysts. *Science* **2012**, *338*, 1434. [CrossRef]
121. Gramage-Doria, R.; Reek, J.N.H. Neues aus der Goldkatalyse–die Größe zählt. New Endeavors in Gold Catalysis—Size Matters. *Angew. Chem.* **2013**, *125*, 13384–13386, New Endeavors in Gold Catalysis—Size Matters. *Angew. Chem. Int. Ed.* **2013**, *52*, 13146–13148. [CrossRef]
122. Blanco Jaimes, M.C.; Bçhling, C.R.N.; Serrano-Becerra, J.M.; Hashmi, A.S.K. Hochaktive einkernige NAC-Gold (I)-Katalysatoren. *Angew. Chem.* **2013**, *125*, 8121–8124, Highly active mononuclear NAC–gold (I) catalysts. *Angew. Chem. Int. Ed.* **2013**, *52*,7963–7966. [CrossRef]
123. Blanco Jaimes, M.C.; Rominger, F.; Pereira, M.M.; Carrilho, R.M.B.; Carabineiroc, S.A.C.; Hashmi, A.S.K. Highly active phosphite gold (I) catalysts for intramolecular hydroalkoxylation, enyne cyclization and furanyne cyclization. *Chem. Commun.* **2014**, *50*, 4937–4940. [CrossRef]
124. Pan, S.; Saha, R.; Mandal, S.; Chattaraj, P. σ-Aromatic cyclic M_3^+ (M = Cu, Ag, Au) clusters and their complexation with dimethyl imidazol-2-ylidene, pyridine, isoxazole, furan, noble gases and carbon monoxide. *Phys. Chem. Chem. Phys.* **2016**, *18*, 11661–11676. [CrossRef]
125. Wang, L.; Xu, J.; Kira, M.; Yan, L.; Xiao, X.; Li, Z. A Stable Cyclic $(R_2SnAu)_3$ Anion Having In-Plane σ-Möbius Aromaticity. *Angew. Chem. Int. Ed.* **2020**, *132*, 1996–2000. [CrossRef]

126. Parida, R.; Reddy, G.N.; Ganguly, A.; Roymahapatra, G.; Chakraborty, A.; Giri, S. On the making of aromatic organometallic superalkali complexes. *Chem. Commun.* **2018**, *54*, 3903–3906. [CrossRef]
127. Li, J.; Li, X.; Sun, L.; Wang, X.; Yuan, L.; Wu, L.; Liu, X.; Wang, Y. Syntheses of Triangular Gold Complexes and Their Applications in Hydroamination Reaction. *Eur. J. Inorg. Chem.* **2021**, *40*, 4230–4237. [CrossRef]
128. Zeng, M.S.; Li, L.; Herzon, S.B. A highly active and air-stable ruthenium complex for the ambient temperature anti-Markovnikov reductive hydration of terminal alkynes. *J. Am. Chem. Soc.* **2014**, *136*, 7058–7067. [CrossRef]
129. Li, G.; Jin, R.-C. Gold nanocluster-catalyzed semihydrogenation: A unique activation pathway for terminal alkynes. *J. Am. Chem. Soc.* **2014**, *136*, 11347–11354. [CrossRef]
130. Radkowski, K.; Sundararaju, B.; Furstner, A. A Functional-Group-Tolerant Catalytic trans Hydrogenation of Alkynes. *Angew. Chem. Int. Ed.* **2013**, *52*, 355–360, Version *Angew. Chem.* **2013**, *125*, 373–378. [CrossRef]
131. Jeddi, N.; Scott, N.; Fairlamb, I. Well-Defined Pd_n Clusters for Cross-Coupling and Hydrogenation Catalysis: New Opportunities for Catalyst Design. *ACS Catal.* **2022**, *12*, 11615–11638. [CrossRef]
132. Karunananda, M.; Mankad, N. E-Selective Semi-Hydrogenation of Alkynes by Heterobimetallic Catalysis. *J. Am. Chem. Soc.* **2015**, *137*, 14598–14601. [CrossRef]
133. Deyris, P.A.; Caneque, T.; Wang, Y.; Retailleau, P.; Bigi, F.; Maggi, R.; Maestri, G.; Malacria, M. Catalytic Semireduction of Internal Alkynes with All-Metal Aromatic Complexes. *ChemCatChem.* **2015**, *7*, 3266–3269. [CrossRef]
134. Fürstner, A. Gold and platinum catalysis—A convenient tool for generating molecular complexity. *Chem. Soc. Rev.* **2009**, *38*, 3208–3221. [CrossRef]
135. Fürstner, A.; Davies, P.W. Catalytic carbophilic activation: Catalysis by platinum and gold π acids. *Angew. Chem. Int. Ed.* **2007**, *46*, 3410–3449. [CrossRef]
136. Fürstner, A. From understanding to prediction: Gold-and platinum-based π-acid catalysis for target oriented synthesis. *Acc. Chem. Res.* **2014**, *47*, 925–938. [CrossRef]
137. Guo, H.; Zheng, Z.L.; Yu, F.; Ma, S.M.; Holuigue, A.; Tromp, D.S.; Elsevier, C.J.; Yu, Y.H. [Pd(Ar-BIAN)(alkene)]-Catalyzed Highly Chemo-, Regio-, and Stereoselective Semihydrogenation of 1, 2-Allenyl Phosphonates and Related Compounds. *Angew. Chem. Int. Ed.* **2006**, *45*, 4997–5000, Version *Angew. Chem.* **2006**, *118*, 5119–5122. [CrossRef] [PubMed]
138. Gomez-Gallego, M.; Sierra, M.A. Kinetic isotope effects in the study of organometallic reaction mechanisms. *Chem. Rev.* **2011**, *111*, 4857–4963. [CrossRef]
139. Monfredini, A.; Santacroce, V.; Deyris, P.A.; Maggi, R.; Bigi, F.; Maestri, G.; Malacria, M. Boosting catalyst activity in cis-selective semi-reduction of internal alkynes by tailoring the assembly of all-metal aromatic tri-palladium complexes. *Dalton Trans.* **2016**, *45*, 15786–15790. [CrossRef] [PubMed]
140. Monfredini, A.; Santacroce, V.; Marchiò, L.; Maggi, R.; Bigi, F.; Maestri, G.; Malacria, M. Semi-Reduction of internal alkynes with prototypical subnanometric metal surfaces: Bridging homogeneous and heterogeneous catalysis with trinuclear all-metal aromatics. *ACS Sustain. Chem. Eng.* **2017**, *5*, 8205–8212. [CrossRef]
141. Serafino, A.; Camedda, N.; Lanzi, M.; Ca', N.; Cera, G.; Maestri, G. Inter/Intramolecular Cascade of 1,6-Enynes Catalyzed by All-Metal Aromatic Tripalladium Complexes and Carboxylic Acids. *J. Org. Chem.* **2021**, *86*, 15433–15452. [CrossRef] [PubMed]
142. Ren, J.; Lan, P.C.; Chen, M.; Zhang, W.; Ma, S. Heterogenization of Trinuclear palladium complex into an anionic metal–organic framework through postsynthetic cation exchange. *Organometallics* **2019**, *38*, 3460–3465. [CrossRef]
143. Lanzi, M.; Cañeque, T.; Marchioò, L.; Maggi, R.; Bigi, F.; Malacria, M.; Maestri, G. Alternative Routes to Tricyclic Cyclohexenes with Trinuclear Palladium Complexes. *ACS Catal.* **2018**, *8*, 144–147. [CrossRef]
144. Cecchini, C.; Lanzi, M.; Cera, G.; Malacria, M.; Maestri, G. Complementary Reactivity of 1, 6-Enynes with All-Metal Aromatic Trinuclear Complexes and Carboxylic Acids. *Synthesis* **2019**, *51*, 1216–1224. [CrossRef]
145. Fürstner, A.; Davies, P.; Gress, T. Cyclobutenes by Platinum-Catalyzed Cycloisomerization Reactions of Enynes. *J. Am. Chem. Soc.* **2005**, *127*, 8244–8245. [CrossRef]
146. Mamane, V.; Gress, T.; Krause, H.; Fürstner, A. Platinum- and Gold-Catalyzed Cycloisomerization Reactions of Hydroxylated Enynes. *J. Am. Chem. Soc.* **2004**, *126*, 8654–8655. [CrossRef] [PubMed]
147. Fu, F.; Xiang, J.; Cheng, H.; Cheng, L.; Chong, H.; Wang, S.; Li, P.; Wei, S.; Zhu, M.; Li, Y. A robust and efficient Pd_3 cluster catalyst for the Suzuki reaction and its odd mechanism. *ACS Catal.* **2017**, *7*, 1860–1867. [CrossRef]
148. Sain, S.; Jain, S.; Srivastava, M.; Vishwakarma, R.; Dwivedi, J. Application of Palladium-Catalyzed Cross-Coupling Reactions in Organic Synthesis. *Curr. Org. Synth.* **2019**, *16*, 1105–1142. [CrossRef]
149. Pan, C.; Liu, M.; Zhang, L.; Wu, H.; Ding, J.; Cheng, J. Palladium catalyzed ligand-free Suzuki cross-coupling reaction. *Catal. Commun.* **2008**, *9*, 508–510. [CrossRef]
150. Diehl, C.J.; Scattolin, T.; Englert, U.; Schoenebeck, F. C–I-Selective Cross-Coupling Enabled by a Cationic Palladium Trimer. *Angew. Chem. Int. Ed.* **2019**, *58*, 211–215. [CrossRef] [PubMed]
151. Scott, N.W.J.; Ford, M.J.; Schotes, C.; Parker, R.R.; Whitwood, A.C.; Fairlamb, I.J.S. The Ubiquitous Cross-Coupling Catalyst System '$Pd(OAc)_2/2PPh_3$ Forms a Unique Dinuclear Pd^I Complex: An Important Entry Point into Catalytically Competent Cyclic Pd_3 Clusters. *Chem. Sci.* **2019**, *10*, 7898–7906. [CrossRef]
152. Li, X.; Li, J.; Wang, X.; Wu, L.; Wang, Y.; Maestri, G.; Malacria, M.; Liu, X. Sulfur and aryl phosphine stabilized aromatic triangular tri-palladium complexes $[Pd_3]^+$: Photoelectric properties and their catalytic applications in the Suzuki–Miyaura reaction. *Dalton Trans.* **2021**, *50*, 11834–11842. [CrossRef]

153. Wang, X.; Sun, L.; Wang, M.; Maestri, G.; Malacria, M.; Liu, X.; Wang, Y.; Wu, L. Sonogashira and Heck coupling reactions catalyzed by $[Pd_3]^+$. *Eur. J. Org. Chem.* **2022**, *2022*, e202200009. [CrossRef]
154. Ma, J.C.; Dougherty, D.A. The cation–π interaction. *Chem. Rev.* **1997**, *97*, 1303–1324. [CrossRef]
155. Meyer, E.A.; Castellano, R.K.; Diederich, F. Interactions with aromatic rings in chemical and biological recognition. *Angew. Chem. Int. Ed.* **2003**, *42*, 1210–1250. [CrossRef]
156. Schottel, B.L.; Chifotides, H.T.; Dunbar, K.R. Anion-π interactions. *Chem. Soc. Rev.* **2008**, *37*, 68–83. [CrossRef] [PubMed]
157. Tsipis, A.C.; Tsipis, C.A. Ligand-stabilized aromatic three-membered gold rings and their sandwichlike complexes. *J. Am. Chem. Soc.* **2005**, *127*, 10623–10638. [CrossRef]
158. Jentzsch, A.V.; Hennig, A.; Mareda, J.; Matile, S. Synthetic ion transporters that work with anion–π interactions, halogen bonds, and anion–macrodipole interactions. *Acc. Chem. Res.* **2013**, *46*, 2791–2800. [CrossRef] [PubMed]
159. Archambault, C.; Bender, R.; Braunstein, P.; Dusausoy, Y.; Welter, R. Reactions of trinuclear platinum clusters with electrophiles: Ionisation isomerism with $[Pt_3(\mu_2\text{-}I)(\mu\text{-}PPh_2)_2(PPh_3)_3]I$ and $[Pt_3\ (\mu\text{-}PPh_2)_2I_2(PPh_3)_3]$. Structures of $[Pt_3(\mu_2\text{-}Cl)(\mu\text{-}PPh_2)_2(PPh_3)_3]PF_6$,$[Pt_3(\mu\text{-}PPh_2)_2I_2(PPh_3)_3]$ and of the Pt–Ag cluster $[Pt_3\{\mu_3\text{-}AgBF_4\}(\mu_2\text{-}I)(\mu\text{-}PPh_2)_2(PPh_3)_3]BF_4$. *Dalton Trans.* **2014**, *43*, 8609–8619. [CrossRef] [PubMed]
160. Bender, R.; Welter, R.; Braunstein, P. Phosphanido-bridged triangular platinum clusters as versatile platforms: A personal account. *Inorganica Chim. Acta* **2015**, *424*, 20–28. [CrossRef]
161. Gamrad, W.; Dreier, A.; Goddard, R.; Porschke, K.R. Cation–Cation Pairing by N–C–H···O Hydrogen Bonds. *Angew. Chem. Int. Ed.* **2015**, *54*, 4482–4487. [CrossRef]
162. Bremer, D.C.M.; von R. Schleyer, P.; Schötz, K.; Kausch, M.; Schindler, M. Four-Center Two-Electron Bonding in a Tetrahedral Topology. Experimental Realization of Three-Dimensional Homoaromaticity in the 1, 3-Dehydro-5, 7-adamantanediyl Dication. *Angew. Chem. Int. Ed.* **1987**, *26*, 761–763. [CrossRef]
163. Wang, Y.; Monfredini, A.; Deyris, P.A.; Blanchard, F.; Derat, E.; Maestri, G.; Malacria, M. All-metal aromatic cationic palladium triangles can mimic aromatic donor ligands with Lewis acidic cations. *Chem. Sci.* **2017**, *8*, 7394–7402. [CrossRef]
164. Czekner, J.; Cheung, L.; Kocheril, G.; Kulichenko, M.; Boldyrev, A.; Wang, L. High-Resolution Photoelectron Imaging of IrB_3^-: Observation of a π-Aromatic B_3^+ Ring Coordinated to a Transition Metal. *Angew. Chem. Int. Ed.* **2019**, *58*, 8877–8881. [CrossRef]
165. Cheung, L.; Czekner, J.; Kocheril, G.; Wang, L. High-resolution photoelectron imaging of MnB_3^-: Probing the bonding between the aromatic B_3 cluster and 3d transition metals. *J. Chem. Phys.* **2020**, *152*, 244306. [CrossRef] [PubMed]
166. Du, Y.; Sheng, H.; Astruc, D.; Zhu, M. Atomically Precise Noble Metal Nanoclusters as Efficient Catalysts: A Bridge between Structure and Properties. *Chem. Rev.* **2020**, *120*, 526–622. [CrossRef] [PubMed]
167. Yao, J.; Bai, J.; Kang, X.; Zhu, M.; Guo, Y.; Wang, X. Non-directed C–H arylation of electron-deficient arenes by synergistic silver and Pd_3 cluster catalysis. *Nanoscale* **2023**, *15*, 3560–3565. [CrossRef] [PubMed]
168. Giner, X.; Najera, C.; Kovacs, G.; Lledos, A.; Ujaqueb, G. Gold versus Silver-Catalyzed Intermolecular Hydroaminations of Alkenes and Dienes. *Adv. Synth. Catal.* **2011**, *353*, 3451–3466. [CrossRef]
169. Bjoremark, P.M.; Olsson, S.; Kokoli, T.; Hakansson, M. Absolute asymmetric synthesis of a tetrahedral silver complex. *Chem. Eur. J.* **2015**, *21*, 8750–8753. [CrossRef] [PubMed]
170. Urnėžius, E.; Brennessel, W.W.; Cramer, C.J.; Ellis, J.E.; Schleyer, P.v.R. A carbon-free sandwich complex $[(P_5)_2Ti]^{2-}$. *Science* **2002**, *295*, 832–834. [CrossRef] [PubMed]
171. Osuga, T.; Murase, T.; Ono, K.; Yamauchi, Y.; Fujita, M. $[m\times n]$ metal ion arrays templated by coordination cages. *J. Am. Chem. Soc.* **2010**, *132*, 15553–15555. [CrossRef] [PubMed]
172. Mercero, J.M.; Piris, M.; Matxain, J.M.; Lopez, X.; Ugalde, J.M. Sandwich complexes of the metalloaromatic η^3-Al_3R_3 ligand. *J. Am. Chem. Soc.* **2009**, *131*, 6949–6951. [CrossRef]
173. Pan, F.X.; Li, L.J.; Wang, Y.J.; Guo, J.C.; Zhai, H.J.; Xu, L.; Sun, Z.M. An all-metal aromatic sandwich complex $[Sb_3Au_3Sb_3]^{3-}$. *J. Am. Chem. Soc.* **2015**, *137*, 10954–10957. [CrossRef]
174. Li, W.; Xu, C.; Hua, S.; Li, J. Theoretical studies on the bonding and electron structures of a $[Au_3Sb_6]^{3-}$ complex and its oligomers. *Dalton Trans.* **2016**, *45*, 11657–11667. [CrossRef]
175. Tang, L.H.; Zhu, T.T.; Ning, P.; Li, K.; Bao, S.Y.; Jin, X.; Zhang, X.Y. Design and structural characterization of the all-metal aromatic sandwich species $[Bi_3Au_3Bi_3]^{3-}$: Insight from density functional theory. *New J. Chem.* **2017**, *41*, 2321–2327. [CrossRef]
176. Peerless, B.; Schmidt, A.; Franzke, Y.; Dehnen, S. φ-Aromaticity in prismatic $\{Bi_6\}$-based clusters. *Nat. Chem.* **2023**, *15*, 347–356. [CrossRef]
177. Zhu, H.; Cao, T.; Zhang, Q.; Liang, X.; Suo, B.; Zou, W.; Han, H.; Huang, Y.; Li, J. All-Metal Aromatic Sandwich Binuclear Complexes: Electronic Structures, Aromaticity and Interactions with Hydrogen via Multicenter Bonds. *ChemistrySelect* **2017**, *2*, 6206–6211. [CrossRef]
178. Zhu, H.; Han, Y.; Suo, B.; Zhai, G.; Wen, Z. All-metal binuclear sandwich complexes $Al_4Ti_2Al_4$: High capacity hydrogen storage through multicenter bonds. *Int. J. Hydrogen Energy* **2017**, *42*, 5440–5446. [CrossRef]
179. Wang, Y.; Feng, L.; Zhai, H. Sandwich-type $Na_6B_7^-$ and $Na_8B_7^+$ clusters: Charge-transfer complexes, four-fold π/σ aromaticity, and dynamic fluxionality. *Phys. Chem. Chem. Phys.* **2019**, *21*, 18338–18345. [CrossRef]
180. Yamaura, H.; Yamamoto, K.; Murahashi, T. Selective dimerization of a trinuclear mixed-metal sandwich complex: Construction of an axially chiral metal skeleton. *Chem. Commun.* **2021**, *57*, 9120–9123. [CrossRef] [PubMed]

181. Benmachiche, A.; Zouchoune, B. Coordination and ligands' effects in trinuclear $[Pd_3(COT)_2(L)]^{2+}$(L = H_2O, CO, N_2, HCN, HNC, NH_3, PH_3, PCl_3, PF_3, CS, CH_2) sandwich complexes of cyclooctatetraene: Theoretical investigation. *Struct. Chem.* **2019**, *30*, 2339–2346. [CrossRef]
182. Jandl, C.; Pankhurst, J.; Love, J.; Pothig, A. Rational Synthesis and Electronic Structure of Functionalized Trinuclear Pd Metal Sheet Sandwich Complexes. *Organometallics* **2017**, *36*, 2772–2783. [CrossRef]